the patients. On the other hand, common phenotypic features can be seen in patients with overlapping interstitial chromosomal deletions but random deletion sizes and random breakpoints. In such cases, the main gene(s) responsible for the common phenotypic features are included in the common deletion region; for example, the methyl-CpG binding domain protein 5 gene (*MBD5*) at 2q23.1 and the myocyte enhancer factor 2C gene (*MEF2C*) at 5q14.3 [Le Meur et al., 2010; Talkowski et al., 2011; Shimojima et al., 2012; Shichiji et al., 2013]. We have previously reported a new chromosomal microdeletion syndrome that is derived from a 5q31.3 deletion and is associated with severe developmental delay and delayed myelination [Shimojima et al., 2011]. After our first report was published, similar cases have been reported, and the shortest region of overlap (SRO) was narrowed down to the 370 kb region [Hosoki et al., 2012].

Interstitial deletions of the short arm of chromosome 3 are rare, and the 3p deletion syndrome is generally indicative of a 3p25 microdeletion that involves the subtelomeric region of 3p [Cargile et al., 2002; Malmgren et al., 2007; Fernandez et al., 2008; Shuib et al., 2009; Pohjola et al., 2010]. There are some patients with interstitial deletions involving 3p25, who showed the core features, including cognitive handicap, growth retardation, microcephaly, and facial dysmorphisms [Gunnarsson and Foyn Bruun, 2010; Peltekova et al., 2012]. Other than the 3p25 microdeletions, interstitial deletions of the proximal 3p have been reported as the consequence of the deletions involving 3p12 region, and some patients with this condition have been reported previously [Petek et al., 2003; Lalli et al., 2007; Tutulan-Cunita et al., 2012]. In comparison, only one patient with a deletion involving 3p21.31 region has been reported by Haldeman-Englert et al. [2009]. In this study, we report two additional cases of the patients with 3p21.31 deletions. These three patients with overlapping deletions of this region share characteristic features, and the newly identified deletion regions narrowed down the SRO. The genes suspected to be responsible for this condition will be discussed in this study.

MATERIALS AND METHODS

Materials

Peripheral blood samples were obtained from patients and their families after obtaining informed consent based on a permission approved by the institution's ethnical committee. DNA was extracted from the peripheral blood samples by using the QIAamp DNA mini kit (Qiagen, Hilden, Germany). For fluorescent in situ hybridization (FISH) analysis, metaphase spreads were prepared from the peripheral blood samples by using the standard method, as previously described [Shimojima et al., 2009, 2010].

Molecular and Cytogenetic Examination

Genomic copy numbers were analyzed by chromosomal microarray testing by using the SurePrint G3 Hmn CGH 60k Oligo Microarray Kit (Agilent Technologies, Santa Clara, CA) as described previously [Shimojima et al., 2009, 2010, 2011, 2012; Shichiji et al., 2013]. Genomic copy number aberrations were visualized using Agilent Genomic Workbench version 6.5 (Agilent Technologies). To confirm the results of the chromosomal microarray testing, FISH analysis was performed using human bacterial artificial chromosomes (BACs) as the probes; RP11-949J7 (3p21.31:49,418,328–49,604,890) and RP11-63O1 (3p26.3:2,468,357–2,644,407), which were selected from the UCSC genome browser (http://www.gwenome.ucsc.edu; GRCh37/hg19).

RESULTS

Genomic Copy Number Aberrations

The overlapping two deletions of 3p21.31 were identified in two independent patients.

Patient 1 showed a loss of genomic copy number with a size of 1.9 Mb, indicated by arr 3p21.31(48,335,484–50,215,391) × 1, and Patient 2 showed a loss of genomic copy with a size of 1.3 Mb, indicated by arr 3p21.31(49,129,830–50,440,305) × 1 (Fig. 1). The genomic locations are referring build19.

Subsequent FISH analyses confirmed simple interstitial deletions in metaphase spreads from both patients (Fig. 2). Since the 3p21.31 deletion was absent in the parents of both patients, the deletions identified in the two independent patients were determined to have de novo origins.

Patient Reports

The clinical features of the present patients are summarized in Table I, along with a comparison to the previously reported patient.

Patient 1

A 26-month-old girl was born at 42 weeks and 2 days of gestation. She had a birth weight of 3,600 g (+1.0 standard deviation [SD]), length of 48 cm (−1.3 SD), and occipitofrontal circumpherence (OFC) of 36 cm (−1.3 SD). Her parents and elder sister were healthy, and the history of the pregnancy period was unremarkable. At the health check-up performed when the patient was 1-month-old, generalized hypotonia and a heart murmur were noted. Echocardiology analysis showed a ventricular septal defect (VSD), which spontaneously closed when the patient was 8 months old. Psychomotor development was mildly delayed, that is, she showed head control at 5 months, rolling over at 6 months, could stand with support at 12 months, and could walk alone at 18 months. There was no history of epilepsy.

At present, her height is 84 cm (−0.6 SD) and weight is 11.2 kg (−0.1 SD). She walks with an ataxic gait. She can understand her parents' verbal suggestions but does not speak any meaningful words. She can use a spoon at mealtime. Use of the Enjoji scale for examination suggests a mild delay with a developmental quotient (DQ) of 60 [Orito et al., 2009]. Brain magnetic resonance imaging (MRI) shows a T2-high intensity area in the deep white matter of the brain (Fig. 3). The T2-high intensity area is predominantly seen in the deep white matter surrounding the posterior horn of the lateral ventricle. Dilated Virchow–Robin spaces are also noted. She shows distinctive facial features, including facial asymmetry, a hypotonic face, arched eyebrows, synophrys, hypertelorism, epicanthus, a flat nasal bridge, an anteverted nostril, a long philtrum, downturned corners of the mouth, micrognathia, low-set ears, and micrognathia

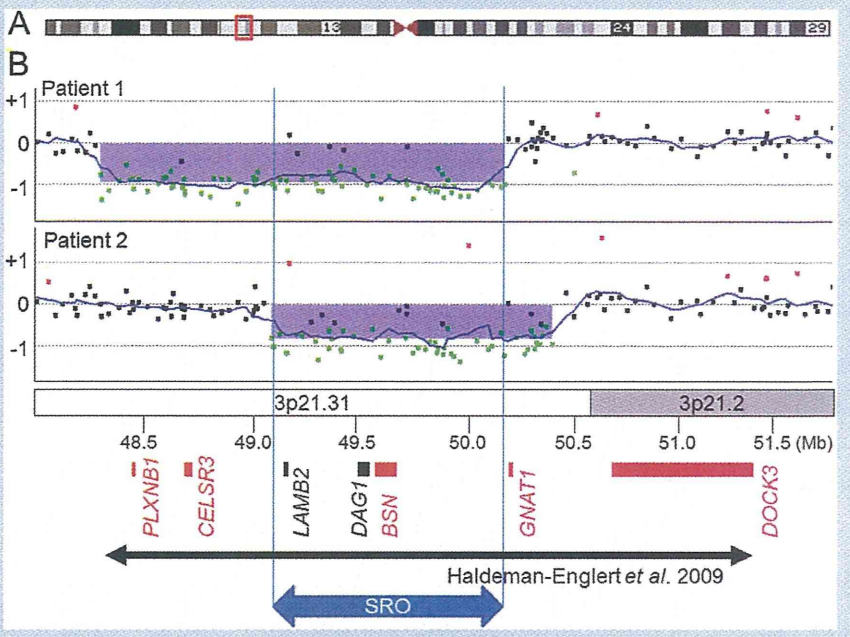

FIG. 1. Results of chromosomal microarray testing and the genome map around 3p21.31. A: Schematic representation of chromosome 3 captured from the UCSC genome browser. The region emphasized by a red rectangle is expanded below. B: The deletion regions of 3p21.31 identified in the two patients (Patient 1 and Patient 2) are focused on and expanded by Gene View of Agilent Genomic Workbench (Agilent Technologies; above). The *x*- and *y*-axes indicate genomic locations (build19) and the $\log_2$ ratio of probe intensity, respectively. Blue translucent rectangles indicate aberration regions. The deletion region reported by Haldeman-Engert et al. and the shortest region of overlap (SRO) are depicted by a black and a blue bars, respectively, with arrows on both sides (bottom). The locations of the genes are indicated by rectangles. Red rectangles indicate the five genes, which were listed as the candidate genes by Haldeman-Engert et al., because of high expression level in the brain. Among them, only *BSN* is included in the SRO. The locations of the genes discussed in the text are also designated by black rectangles.

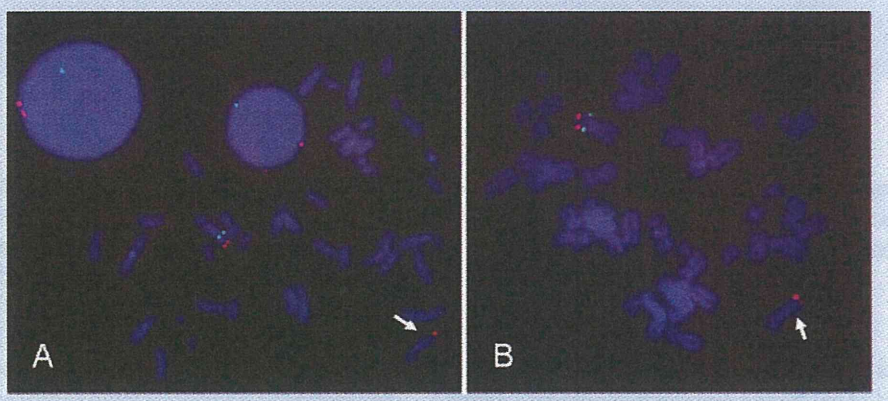

FIG. 2. Results FISH analyses. Patient 1 (A) and Patient 2 (B). Red signals of RP11-6301 (3p26.3) are the marker of chromosome 3. Green signals for RP11-949J7 (3p21.31) can be detected in one of the chromosome 3 regions in both patients, indicating deletions of this region (arrow).

TABLE I. The Clinical Features of the Patients

	Haldeman-Ehglert	Patient 1	Patient 2
Birth			
Gestational weeks	38 weeks	42 weeks	38 weeks
Weight	2,200 g (<5th centile)	3,600 g	3,505 g
OFC	NA	36 cm	35.4 cm
Growth			
Grwoth delay	+	−	+
Short stature	+	−	+
Microcephaly	−	−	−
Dysmorphism			
Facial asymmetry	−	+	−
Broad forehead	+	+	−
Arched eyebrows	+	+	+
Synophrys	NA	+	−
Hypertelorism	+	+	+
Epicunthas	+	+	+
Upslanting palpebral fissure	+	−	+
Flat nasal bridge	NA	+	−
Anteverted nostril	NA	+	−
Bulbous nasal tip	+	+	−
Long philtrum	+	+	−
Cleft lip	+	−	−
Cleft soft palate	−	−	+
Downturned corners of the mouth	NA	+	−
Micrognathia	+	+	+
Low set ears	NA	+	−
Widely-spaced nipples	+	−	−
Neurological			
Developmental delay	+	+	+
Hypotonia	+	+	+
Hypotonic-appearing facies	+	+	−
Cortical blindness	+	−	−
Pale fundi	+	−	−
Partial agenesis of the corpus callosum	+	−	−
Seizure	+	−	−
Abnormal EEG	+	−	−
Gastroesophageal reflux	+	−	−
Abnormal signals in brain MRI	NA	+	+
Others			
Congenital heart anomaly	−	VSD (spontaneous closure)	ASD + PDA

NA, not available.

(Fig. 4A). The first fingers on both hands are broad and the other fingers are short and narrow. Blood examination showed an elevated serum creatine kinase (CK) level of 1,075 U/L.

Patient 2

A 15-year-old girl was born at 38 weeks of gestation by a cesarean. She is the second child of healthy and nonconsanguineous parents. Her birth weight was 3,505 g (+1.4 SD). Her 17-year-old brother had a past history of West syndrome in infancy and now has a pervasive developmental disorder. He showed no abnormality on conventional G-banding and chromosomal microarray testing. Although there was no complication during gestation, the patient experienced feeding difficulties due to hypotonia and laryngomalacia in her early infancy. Hypocalcemia was also noted at that time. Psychomotor development was delayed; for example, she showed head control at 9 months, could sit at 18 months, walk without support at 30 months, and could speak the first word at 18 months. When she was 3 years old, psychomotor delay was suggested. She had recurrent acute otitis media and an episode of a febrile seizure in her childhood. At 6 years, nasopharyngeal regurgitation was detected. At 7 years, an atrial septal defect (ASD) and patent ductus arteriosus (PDA) were diagnosed and surgically repaired. Due to a growth hormone (GH) deficiency, which was diagnosed at 11 years,

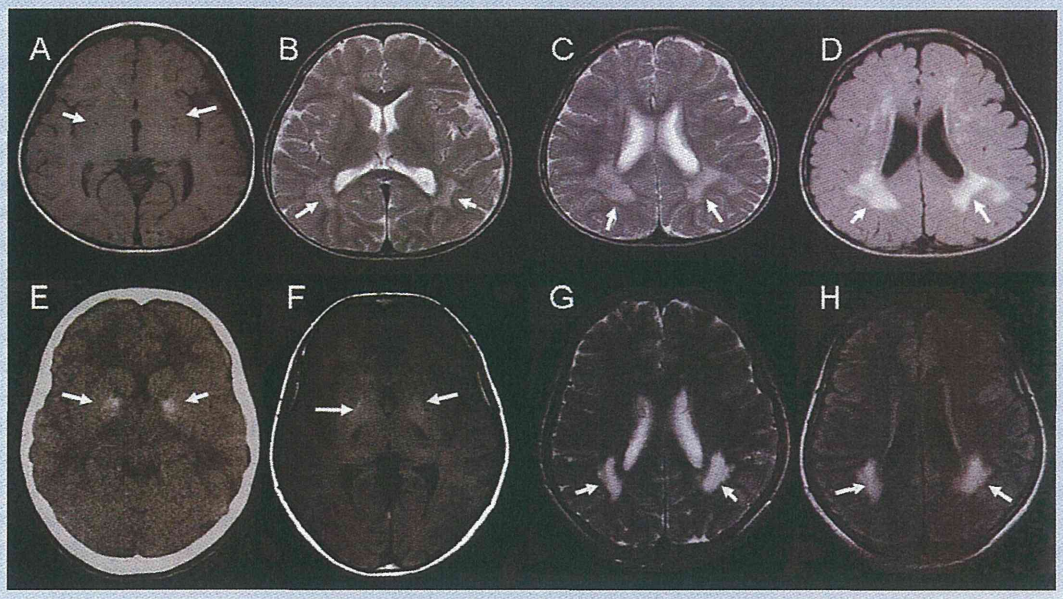

FIG. 3. Images of the brain radiological examinations. A–D: Axial images of brain MRI examined when Patient 1 was 26 months old. A: T1-weighted image indicates low-intensity areas in the basal nucleus, indicating dilated Virchow–Robin spaces (arrows). T2-weighted (B,C) and FLAIR (D) images indicate abundant high-intensity areas in the white matter (arrows). E: Cranial CT image examined when Patient 2 was 12 years old shows the finding of calcifications in the basal nucleus (arrows). F–H: Axial images of brain MRI examined when Patient 2 was 14 years old. F: T1-weighted image indicates high-intensity areas in the basal nucleus (arrows). T2-weighted (G) and FLAIR (H) images indicate occipital-dominant high-intensity areas in the white matter (arrows).

GH replacement therapy was initiated. At 14 years, atomoxetine was prescribed for the patient's behavioral problems related to attention-deficit/hyperactivity disorder.

When the patient was 12 years old, brain computed tomography (CT) was performed, and mild calcification was noted at the pallidum on both sides (Fig. 3). Brain MRI performed when the patient was 14 years old showed an abnormal-intensity area, that is, T1-high intensity in the basal nucleus on both sides (internal putamen and pallidum) and T2-/fluid-attenuated inversion recovery (FLAIR) high intensity in the posterior deep periventricular white matter on both sides (Fig. 3). At 15 years, her DQ was examined by the Kyoto Scale of Psychological Development 2001 and the score was 38, indicating moderate intellectual disability. Chromosomal G-banding showed a normal female karyotype of 46,XX.

At present, she shows short stature; with a height of 144.5 cm (−2.3 SD), a weight of 33.8 kg (−2.1 SD), and OFC of 53.5 cm (−0.4 SD). Her facial features are distinctive with arched-busy eyebrows,

FIG. 4. Facial appearance of both patients. Patient 1 (A) shows facial asymmetry, flat nasal bridge, anteverted nostrils, a long philtrum, downslanting mouth corners, and micrognathia. At 2 years of age (B), Patient 2 shows arched eyebrows, prominent eyelashes, hypertelorism, epicanthus, a narrow nasal base, and micrognathia. Patient 2 at 15 years of age (C).

prominent eyelashes, hypertelorism, epicanthus, a narrow nasal base, a low nasal bridge, and macro incisors (Fig. 4C). These features mimicked those of 22q11.2 deletion syndrome, but FISH analysis targeted for the 22q11.2 region yielded negative results. Neurological examination showed muscle hypotonia. Blood examination showed a mildly elevated serum CK level of 465 U/L.

DISCUSSION

In this study, we identified two overlapping interstitial chromosomal deletions of 3p21.31 in two independent patients. Each patient showed common phenotypic features, including developmental delay, hypotonia, distinctive facial features, an elevated serum CK level, and characteristic white matter involvement. The two identified deletions overlapped with that detected in the patient reported by Haldeman-Englert et al. [2009]. Although the developmental delay and hypotonia seen in the three patients with the 3p21.31 deletions are common findings in patients with chromosomal aberrations, the distinctive facial features (e.g., arched eyebrows, hypertelorism, epicanthus, and micrognathia) would be a characteristic of patients with 3p21.31 deletions (Fig. 4).

The most striking finding of the two patients identified in this study was white matter involvement, which was revealed by brain MRI. T2 and FLAIR MRI of the brain showed high-intensity areas in the white matter, especially in the deep white matter surrounding the dorsal horns of the ventricles. This finding may indicate hypomyelination of the neural tracts. Patient 2 showed additional neuroradiological findings, including a T1-weighted high-intensity area in the basal nucleus seen in brain MRI and calcifications suggested by brain CT. These findings may be age dependent because the patient reported by Haldeman-Englert et al. [2009] did not show any abnormal findings on brain MRI at the age of 7 months.

Haldeman-Englert et al. [2009] had discussed the genes which may be responsible for their patient's neurological features, and five genes had been listed as the candidate genes (Fig. 1); the plexin B1 gene (*PLXNB1*), the cadherin EGF LAG seven-pass G-type receptor 3 gene (*CELSR3*), the bassoon (presynaptic cytomatrix protein) gene (*BSN*), the guanine nucleotide binding protein (G protein) alpha transducing activity polypeptide 1 gene (*GNAT1*), and the dedicator of cytokinesis 3 gene (*DOCK3*). In this study, the two identified deletions narrowed down the SRO of the 3p21.31 deletions to within 1 Mb (chr3:49,129,830-50,215,391) by the centromeric and telomeric ends of the deletions identified in Patients 1 and 2, respectively (Fig. 1). Although this region is gene rich and a total of 38 genes are still included (Supplemental eTable SI), only *BSN*, from among the five candidate genes proposed by Haldeman-Englert et al., was included in SRO (Fig. 1). Bassoon encoded by *BSN* is thought to be involved in cytomatrix organization at the active zones of synapses [tom Dieck et al., 1998]. Mice knockout bassoon showed no abnormalities in synapse density and morphological parameters, but synaptic transmission was reduced and short-term synaptic depression was enhanced [Altrock et al., 2003; Hallermann et al., 2010]. Neuroradiological findings with white matter involvement detected in the present two patients were quite unique. Thus, *BSN* haploinsufficiency may be related to the neurological and neuroradiological features of the patients with microdeletions of 3p21.31, although no direct evidence is available in this regard. More information would be needed to establish a clear genotype-phenotype correlation.

The other important genes included in SRO are the laminin beta 2 gene (*LAMB2*) and the dystrophin-associated glycoprotein 1 gene (*DAG1*; Fig. 1). *LAMB2* encodes one of the components of laminins, which are multidomain heterotrimeric glycoproteins of the basal lamina contain some chains, and is expressed at the neuromuscular junctions. Cortical dysplasia has been observed in the mice lacking laminin chains [Radner et al., 2013], although *LAMB2* is responsible for an autosomal recessive congenital nephrotic syndrome, Pierson syndrome (OMIM#609049) [Zenker et al., 2004]. On the other hand, *DAG1* is required on the end feet of radial glia, and the zebrafish *dag1* mutant has been reported to show brain abnormalities and ocular defects reminiscent of the phenotypes observed in the human condition known as muscle-eye-brain disease [Gupta et al., 2011; Myshrall et al., 2012]. Recently, a homozygous mutation of *DAG1* was identified in a patient with limb-girdle muscular dystrophy and cognitive impairment [Hara et al., 2011]. Because these genes have functions in muscle and neuromuscular junctions, haploinsufficiencies of these genes may be related to hypotonia commonly seen in the patients with microdeletions of 3p21.31 and elevated serum CK levels, which were specifically seen in the two patients in this study.

Regarding the other clinical features, the two patients of this study showed congenital heart defects, including VSD and ASD + PDA. However, the patient reported by Haldeman-Englert et al. [2009] did not show any congenital heart defects. Short stature was evident in Patient 2 in the present study and the patient reported by Haldeman-Englert et al. [2009]. Because Patient 1 in this study also showed mildly affected short stature, it is possible that this finding may be frequently seen in patients with microdeletions of 3p21.31.

In this study, we confirmed common phenotypic features in the patients with microdeletions of 3p21.31 and identified additional features that have not been reported previously. Because the constellation of such characteristic features is quite unique, clinical manifestations of the patients with microdeletions of 3p21.31 would be clinically recognizable as a contiguous gene deletion syndrome.

ACKNOWLEDGMENTS

We would like to express our gratitude to the patients and their families for their cooperation. This work was partially supported by a Grant-in-Aid for Scientific Research on Innovative Areas "Foundation of Synapse and Neurocircuit Pathology" from the Ministry of Education, Culture, Sports, Science and Technology (MEXT; T.Y.); a Grant-in-Aid for Scientific Research from Health Labor Sciences Research Grants from the Ministry of Health, Labor, and Welfare, Japan (T.Y.).

REFERENCES

Altrock WD, tom Dieck S, Sokolov M, Meyer AC, Sigler A, Brakebusch C, Fassler R, Richter K, Boeckers TM, Potschka H, Brandt C, Loscher W, Grimberg D, Dresbach T, Hempelmann A, Hassan H, Balschun D, Frey JU, Brandstatter JH, Garner CC, Rosenmund C, Gundelfinger ED. 2003.

Functional inactivation of a fraction of excitatory synapses in mice deficient for the active zone protein bassoon. Neuron 37:787–800.

Cargile CB, Goh DL, Goodman BK, Chen XN, Korenberg JR, Semenza GL, Thomas GH. 2002. Molecular cytogenetic characterization of a subtle interstitial del(3)(p25.3p26.2) in a patient with deletion 3p syndrome. Am J Med Genet 109:133–138.

Fernandez TV, Garcia-Gonzalez IJ, Mason CE, Hernandez-Zaragoza G, Ledezma-Rodriguez VC, Anguiano-Alvarez VM, E'Vega R, Gutierrez-Angulo M, Maya ML, Garcia-Bejarano HE, Gonzalez-Cruz M, Barrios S, Atorga R, Lopez-Cardona MG, Armendariz-Borunda J, State MW, Davalos NO. 2008. Molecular characterization of a patient with 3p deletion syndrome and a review of the literature. Am J Med Genet Part A 146A:2746–2752.

Gunnarsson C, Foyn Bruun C. 2010. Molecular characterization and clinical features of a patient with an interstitial deletion of 3p25.3–p26.1. Am J Med Genet Part A 152A:3110–3114.

Gupta V, Kawahara G, Gundry SR, Chen AT, Lencer WI, Zhou Y, Zon LI, Kunkel LM, Beggs AH. 2011. The zebrafish dag1 mutant: A novel genetic model for dystroglycanopathies. Hum Mol Genet 20:1712–1725.

Haldeman-Englert CR, Gai X, Perin JC, Ciano M, Halbach SS, Geiger EA, McDonald-McGinn DM, Hakonarson H, Zackai EH, Shaikh TH. 2009. A 3.1-Mb microdeletion of 3p21.31 associated with cortical blindness, cleft lip, CNS abnormalities, and developmental delay. Eur J Med Genet 52:265–268.

Hallermann S, Fejtova A, Schmidt H, Weyhersmuller A, Silver RA, Gundelfinger ED, Eilers J. 2010. Bassoon speeds vesicle reloading at a central excitatory synapse. Neuron 68:710–723.

Hara Y, Balci-Hayta B, Yoshida-Moriguchi T, Kanagawa M, Beltran-Valero de Bernabe D, Gundesli H, Willer T, Satz JS, Crawford RW, Burden SJ, Kunz S, Oldstone MB, Accardi A, Talim B, Muntoni F, Topaloglu H, Dincer P, Campbell KP. 2011. A dystroglycan mutation associated with limb-girdle muscular dystrophy. N Engl J Med 364:939–946.

Hosoki K, Ohta T, Natsume J, Imai S, Okumura A, Matsui T, Harada N, Bacino CA, Scaglia F, Jones JY, Niikawa N, Saitoh S. 2012. Clinical phenotype and candidate genes for the 5q31.3 microdeletion syndrome. Am J Med Genet Part A 158A:1891–1896.

Koolen DA, Sharp AJ, Hurst JA, Firth HV, Knight SJ, Goldenberg A, Saugier-Veber P, Pfundt R, Vissers LE, Destree A, Grisart B, Rooms L, Van der Aa N, Field M, Hackett A, Bell K, Nowaczyk MJ, Mancini GM, Poddighe PJ, Schwartz CE, Rossi E, De Gregori M, Antonacci-Fulton LL, McLellan MD II, Garrett JM, Wiechert MA, Miner TL, Crosby S, Ciccone R, Willatt L, Rauch A, Zenker M, Aradhya S, Manning MA, Strom TM, Wagenstaller J, Krepischi-Santos AC, Vianna-Morgante AM, Rosenberg C, Price SM, Stewart H, Shaw-Smith C, Brunner HG, Wilkie AO, Veltman JA, Zuffardi O, Eichler EE, de Vries BB. 2008. Clinical and molecular delineation of the 17q21.31 microdeletion syndrome. J Med Genet 45:710–720.

Lalli C, Galasso C, Lo Castro A, Nardone AM, Di Paolo A, Curatolo P. 2007. Interstitial deletion of a proximal 3p: A clinically recognisable syndrome. Brain Dev 29:312–316.

Le Meur N, Holder-Espinasse M, Jaillard S, Goldenberg A, Joriot S, Amati-Bonneau P, Guichet A, Barth M, Charollais A, Journel H, Auvin S, Boucher C, Kerckaert JP, David V, Manouvrier-Hanu S, Saugier-Veber P, Frebourg T, Dubourg C, Andrieux J, Bonneau D. 2010. MEF2C haploinsufficiency caused by either microdeletion of the 5q14.3 region or mutation is responsible for severe mental retardation with stereotypic movements, epilepsy and/or cerebral malformations. J Med Genet 47: 22–29.

Malmgren H, Sahlen S, Wide K, Lundvall M, Blennow E. 2007. Distal 3p deletion syndrome: Detailed molecular cytogenetic and clinical characterization of three small distal deletions and review. Am J Med Genet Part A 143A:2143–2149.

Myshrall TD, Moore SA, Ostendorf AP, Satz JS, Kowalczyk T, Nguyen H, Daza RA, Lau C, Campbell KP, Hevner RF. 2012. Dystroglycan on radial glia end feet is required for pial basement membrane integrity and columnar organization of the developing cerebral cortex. J Neuropathol Exp Neurol 71:1047–1063.

Orito Y, Oku H, Kubota S, Amino N, Shimogaki K, Hata M, Manki K, Tanaka Y, Sugino S, Ueta M, Kawakita K, Nunotani T, Tatsumi N, Ichihara K, Miyauchi A, Miyake M. 2009. Thyroid function in early pregnancy in Japanese healthy women: Relation to urinary iodine excretion, emesis, and fetal and child development. J Clin Endocrinol Metab 94:1683–1688.

Peltekova IT, Macdonald A, Armour CM. 2012. Microdeletion on 3p25 in a patient with features of 3p deletion syndrome. Am J Med Genet Part A 158A:2583–2586.

Petek E, Windpassinger C, Simma B, Mueller T, Wagner K, Kroisel PM. 2003. Molecular characterisation of a 15 Mb constitutional de novo interstitial deletion of chromosome 3p in a boy with developmental delay and congenital anomalies. J Hum Genet 48:283–287.

Pohjola P, de Leeuw N, Penttinen M, Kaariainen H. 2010. Terminal 3p deletions in two families—Correlation between molecular karyotype and phenotype. Am J Med Genet Part A 152A:441–446.

Radner S, Banos C, Bachay G, Li YN, Hunter DD, Brunken WJ, Yee KT. 2013. β2 and γ3 laminins are critical cortical basement membrane components: ablation of Lamb2 and Lamc3 genes disrupts cortical lamination and produces dysplasia. Dev Neurobiol 73:209–229.

Shichiji M, Ito Y, Shimojima K, Nakamu H, Oguni H, Osawa M, Yamamoto T. 2013. A cryptic microdeletion including MBD5 occurring within the breakpoint of a reciprocal translocation between chromosomes 2 and 5 in a patient with developmental delay and obesity. Am J Med Genet Part A 161:850–855.

Shimojima K, Komoike Y, Tohyama J, Takahashi S, Paez MT, Nakagawa E, Goto Y, Ohno K, Ohtsu M, Oguni H, Osawa M, Higashinakagawa T, Yamamoto T. 2009. TULIP1 (RALGAPA1) haploinsufficiency with brain development delay. Genomics 94:414–422.

Shimojima K, Inoue T, Hoshino A, Kakiuchi S, Watanabe Y, Sasaki M, Nishimura A, Takeshita-Yanagisawa A, Tajima G, Ozawa H, Kubota M, Tohyama J, Sasaki M, Oka A, Saito K, Osawa M, Yamamoto T. 2010. Comprehensive genetic analyses of PLP1 in patients with Pelizaeus-Merzbacher disease applied by array-CGH and fiber-FISH analyses identified new mutations and variable sizes of duplications. Brain Dev 32:171–179.

Shimojima K, Isidor B, Le Caignec C, Kondo A, Sakata S, Ohno K, Yamamoto T. 2011. A new microdeletion syndrome of 5q31.3 characterized by severe developmental delays, distinctive facial features, and delayed myelination. Am J Med Genet Part A 155A:732–736.

Shimojima K, Okumura A, Mori H, Abe S, Ikeno M, Shimizu T, Yamamoto T. 2012. De novo microdeletion of 5q14.3 excluding MEF2C in a patient with infantile spasms, microcephaly, and agenesis of the corpus callosum. Am J Med Genet Part A 158A:2272–2276.

Shinawi M, Liu P, Kang SH, Shen J, Belmont JW, Scott DA, Probst FJ, Craigen WJ, Graham BH, Pursley A, Clark G, Lee J, Proud M, Stocco A, Rodriguez DL, Kozel BA, Sparagana S, Roeder ER, McGrew SG, Kurczynski TW, Allison LJ, Amato S, Savage S, Patel A, Stankiewicz P, Beaudet AL, Cheung SW, Lupski JR. 2010. Recurrent reciprocal 16p11.2 rearrangements associated with global developmental delay, behavioural problems, dysmorphism, epilepsy, and abnormal head size. J Med Genet 47:332–341.

Shuib S, McMullan D, Rattenberry E, Barber RM, Rahman F, Zatyka M, Chapman C, Macdonald F, Latif F, Davison V, Maher ER. 2009. Microarray based analysis of 3p25–p26 deletions (3p– syndrome). Am J Med Genet Part A 149A:2099–2105.

Slavotinek AM. 2008. Novel microdeletion syndromes detected by chromosome microarrays. Hum Genet 124:1–17.

Talkowski ME, Mullegama SV, Rosenfeld JA, van Bon BW, Shen Y, Repnikova EA, Gastier-Foster J, Thrush DL, Kathiresan S, Ruderfer DM, Chiang C, Hanscom C, Ernst C, Lindgren AM, Morton CC, An Y, Astbury C, Brueton LA, Lichtenbelt KD, Ades LC, Fichera M, Romano C, Innis JW, Williams CA, Bartholomew D, Van Allen MI, Parikh A, Zhang L, Wu BL, Pyatt RE, Schwartz S, Shaffer LG, de Vries BB, Gusella JF, Elsea SH. 2011. Assessment of 2q23.1 microdeletion syndrome implicates MBD5 as a single causal locus of intellectual disability, epilepsy, and autism spectrum disorder. Am J Hum Genet 89:551–563.

tom Dieck S, Sanmarti-Vila L, Langnaese K, Richter K, Kindler S, Soyke A, Wex H, Smalla KH, Kampf U, Franzer JT, Stumm M, Garner CC, Gundelfinger ED. 1998. Bassoon, a novel zinc-finger CAG/glutamine-repeat protein selectively localized at the active zone of presynaptic nerve terminals. J Cell Biol 142:499–509.

Tutulan-Cunita AC, Papuc SM, Arghir A, Rotzer KM, Deshpande C, Lungeanu A, Budisteanu M. 2012. 3p interstitial deletion: Novel case report and review. J Child Neurol 27:1062–1066.

Zenker M, Aigner T, Wendler O, Tralau T, Muntefering H, Fenski R, Pitz S, Schumacher V, Royer-Pokora B, Wuhl E, Cochat P, Bouvier R, Kraus C, Mark K, Madlon H, Dotsch J, Rascher W, Maruniak-Chudek I, Lennert T, Neumann LM, Reis A. 2004. Human laminin beta2 deficiency causes congenital nephrosis with mesangial sclerosis and distinct eye abnormalities. Hum Mol Genet 13:2625–2632.

SUPPORTING INFORMATION

Additional supporting information may be found in the online version of this article at the publisher's web-site.

TABLE SI. Gene List Included in SRO

Gene 534 (2014) 144–154

Contents lists available at ScienceDirect

Gene

journal homepage: www.elsevier.com/locate/gene

Late-onset Krabbe disease is predominant in Japan and its mutant precursor protein undergoes more effective processing than the infantile-onset form

Mohammad Arif Hossain [a], Takanobu Otomo [a,1], Seiji Saito [b], Kazuki Ohno [c,2], Hitoshi Sakuraba [d], Yusuke Hamada [a], Keiichi Ozono [a], Norio Sakai [a,*]

[a] Department of Pediatrics, Osaka University Graduate School of Medicine, Suita, Osaka, Japan
[b] Department of Medical Management and Informatics, Hokkaido Information University, Ebetsu, Hokkaido, Japan
[c] NPO for the Promotion of Research on Intellectual Property Tokyo, Chiyoda-ku, Tokyo, Japan
[d] Department of Clinical Genetics, Meiji Pharmaceutical University, Kiyose, Tokyo, Japan

ARTICLE INFO

Article history:
Accepted 8 November 2013
Available online 16 November 2013

Keywords:
Krabbe disease
Globoid cell leukodystrophy
Galactocerebrosidase
Psychosine
Protein processing
Phenotype

ABSTRACT

Krabbe disease is an autosomal recessive leukodystrophy caused by the deficiency of the galactocerebrosidase (GALC) enzyme. It is pathologically characterized by demyelination of the central and peripheral nervous systems by accumulation of galactosylsphingosine. To date, more than 120 mutations in the GALC gene have been reported worldwide and genotype–phenotype correlations have been reported in some types of mutations. In this study, we analyzed 22 unreported Japanese patients with Krabbe disease and summarized a total of 51 Japanese patients, including 29 previously reported patients. To elucidate how GALC mutations impair enzymatic activity, multiple disease-causing mutations including common mutations and polymorphisms were investigated for enzymatic activity and precursor processing ability with transient expression system. We also performed 3-D enzyme structure analysis to determine the effect of each new mutation. Five novel mutations were detected including one deletion c.1808delT [p.L603X], one nonsense mutation c.1023C>G [p.Y341X], and three missense mutations c.209T>C [p.L70P], c.1054G>A [p.G352R], and c.1937G>C [p.G646A]. For the total of 51 patients, 59% had late-onset forms of Krabbe disease. Seven common mutations accounted for 58% of mutant alleles of patients with Krabbe disease in Japan. Infantile-onset mutations had almost no enzyme activity, while late-onset mutations had 4%–20% of normal enzyme activity. The processing rate of precursor GALC protein to mature form was slower for infantile-onset mutations. Heat stability of the mutant proteins revealed that p.G270D was more stable compared to the other mutations. The constructed 3D-model showed that the residues for Krabbe mutations were less solvent-accessible and located in the core region of GALC protein. In conclusion, we have demonstrated that the most common phenotype in Japan is the late-onset type, that the enzyme activity for GALC mutants is correlated with mutational severity, and that the most pathogenic factor is due to the processing rate from the precursor to the mature protein.

1. Introduction

Krabbe disease (globoid cell leukodystrophy; OMIM ID #245200) is an autosomal recessive neurodegenerative disorder caused by a deficiency of galactocerebrosidase (GALC) (EC 3.2.1.46). GALC enzymatic activity is predominantly targeted in lysosomes, where it is essential for normal catabolism of galactolipids, including a major myelin component, galactocerebroside, and psychosine. GALC deficiency results in abnormal accumulation of galactosylsphingosine (psychosine), which is cytotoxic to oligodendrocytes and Schwann cells (Nagara et al., 1986; Tanaka et al., 1988). Loss of these myelin-forming cells causes demyelination in both the central and peripheral nervous systems during early developmental stages (Kobayashi et al., 1988; Seitelberger, 1981). According to the "psychosine hypothesis", the main disease

Abbreviations: ASA, solvent-accessible surface area; BMT, bone marrow transplantation; GALC, galactocerebrosidase; GalCer, galactocerebroside; HM-gal, 6-hexadecanoylamino-4-methylumbelliferyl-β-D-galactopyranoside; RMSD, root-mean-square distance; TIM, central triosephosphate isomerase.

* Corresponding author at: Department of Pediatrics, Osaka University Graduate School of Medicine, 2-2 Yamada-oka, Suita, Osaka 565-0871, Japan. Tel.: +81 6 6879 3932; fax: +81 6 6879 3939.
E-mail address: norio@ped.med.osaka-u.ac.jp (N. Sakai).
[1] Present address: Department of Biochemistry, Children's Hospital, University Medical Center Hamburg-Eppendorf, Hamburg, Germany.
[2] Present address: Drug Discovery Research, Astellas Pharm Inc., Tsukuba, Japan.

0378-1119/$ – see front matter © 2013 Elsevier B.V. All rights reserved.
http://dx.doi.org/10.1016/j.gene.2013.11.003

pathology depends on psychosine accumulation and its degradation rate (Suzuki, 1998).

It has been reported that 90% of patients have the infantile form of the disease with symptoms starting before 6 months of age. The remaining 10% have late-onset forms of Krabbe disease, which are classified into one of three classes, late-infantile (7 months to 3 years), juvenile (3–8 years), or adult (≥9 years) types, depending on the time of disease onset (Wenger et al., 2013). However, Duffner and colleagues recently reported that the incidence of the infantile-onset of the disease was somewhat lower at 62% in the world-wide registry of patients with Krabbe disease (Duffner et al., 2012).

Molecular cloning of the human *GALC* gene by two groups (Chen et al., 1993a; Sakai et al., 1994a) (GenBank Accession Nos. L23116 and L38544, L38559) has led to molecular-level analyses of Krabbe disease. According to the Human Gene Mutation Database (HGMD) more than 120 disease-causing mutations have been identified in the *GALC* gene, many of which occur in compound heterozygous patterns in patients (De Gasperi et al., 1996; Debs et al., 2013; Fu et al., 1999; Furuya et al., 1997; Lissens et al., 2007; Puckett et al., 2012; Selleri et al., 2000; Tappino et al., 2010; Wenger et al., 1997; Wenger et al., 2000). Some genotype–phenotype correlations have been reported for patients with Krabbe disease globally (Wenger et al., 1997) and by our group specifically for Japanese patients (Xu et al., 2006).

A high incidence of polymorphic changes with apparent disease-causing alleles also complicates the interpretation of the effects of mutations. Among them p.I546T and p.I289V are common (mean allele frequency 0.4428 and 0.1108, respectively) [NCBI SNP database]. It has been reported that p.I66M in wild-type *GALC* shows normal enzyme activity but exhibits low enzyme activity when it is associated with the p.I289V polymorphism (Furuya et al., 1997). Other reports have also noted that the presence of the p.I546T polymorphism with some mutations causes low enzyme activity (Harzer et al., 2002; Lissens et al., 2007; Luzi et al., 1996).

The precursor form of GALC contains 685 amino acids (80 kDa) and is processed in lysosomes into two fragments, an *N*-terminal fragment (50 kDa) and a *C*-terminal fragment (30 kDa) (active GALC) (Nagano et al., 1998), and enzyme activity depends on the amount of processed protein from the precursor (Chen and Wenger, 1993). Our group has reported that the optimal pH for purified GALC is 4.2 in the taurocholate system (Sakai et al., 1994b).

In this study, we summarize the genotypes and phenotypes of 51 Japanese patients with Krabbe disease, the largest study so far, which included 22 previously unreported and 29 previously reported patients. To elucidate how *GALC* mutations impair enzymatic activity, we investigated multiple disease-causing mutations including common mutations and polymorphisms for enzymatic activity and precursor processing ability using a transient expression system, and potential correlations between infantile onset and late-onset phenotypes. We used 3-D enzyme structure analysis following the crystal structure of murine precursor GALC (Deane et al., 2011) to determine the effect of each new mutation identified in the previously unreported patients.

2. Materials and methods

2.1. Patients

The study included 22 Japanese patients with newly diagnosed Krabbe disease, who have not been previously reported. Their diagnosis was based on clinical signs, symptoms, and radiological findings with laboratory confirmation based on their low GALC activity in blood lymphocytes and/or skin fibroblasts (Table 1). An additional 29 Japanese patients with Krabbe disease were included, who have been previously reported (Table 2).

With respect to mutation nomenclature, it is recommended to follow the guidelines, which suggest using the first ATG as translation initiation codon as nucleotide +1 (http://www.hgvs.org/mutnomen). However, GALC mutations have been previously reported with the second ATG as nucleotide +1 (Wenger et al., 2000; Xu et al., 2006). We have used the older nucleotide and amino acid numbers in this manuscript and described all mutations with both systems in Table 3.

2.2. Genomic DNA analysis by direct sequencing

After informed consent was obtained, genomic DNA was prepared by standard methods from patients' peripheral blood lymphocytes or cultured skin fibroblasts and used for the subsequent studies. PCR reactions and direct sequencing were conducted as previously described (Xu et al., 2006).

2.3. Screening for the 30-kb deletion mutation

The presence of the 30-kb deletion mutation, which is most dominant in Caucasian patients, was checked using the method previously described by Xu et al. (2006) for patients 1, 3, 4, 14, 16, 17, 20, and 22, who carried only one mutation.

2.4. Screening for p.L70P, p.G352R, and p.G646A in healthy subjects

Genomic DNA from 100 healthy control subjects was screened for restriction fragment length polymorphisms for three novel missense mutations p.L70P, p.G352R, and p.G646A. To detect p.L70P (c.209T>C), genomic DNA samples were amplified using a mismatch-sense primer of exon 2 (5′-TATCGTTCTCAGATATTGGAAGATC) and an antisense primer (Xu et al., 2006). The product was digested with *Bgl*II. To detect p.G352R (c.1054G>A), genomic DNA samples were amplified using a sense primer of exon 10 (Xu et al., 2006) and a mismatch-antisense (5′-TAAGCCATCAGTCAGAGCTACGTAGGATC) primer. The product was digested with *BamH*I. Screening of p.G646A (c.1937G>C) genomic DNA samples was amplified with the primer pair of exon 17 (Xu et al., 2006) and the product was digested with *Bst*NI.

2.5. Cloning and construction of expression vector for human GALC

Wild-type human *GALC* cDNA containing 19-bp upstream from the real first ATG translation initiation site (Sakai et al., 1998) to the *Ase*I site (178-bp downstream from the stop codon) was constructed in a pSVL vector (Amersham). Twelve mutations and polymorphisms were introduced by PCR-based mutagenesis including c.635_646delinsCTC, p.I66M, p.L70P, p.G270D, p.I289V, p.Y341X, p.G352R, p.G496S, p.I546T, p.G569S, p.L618S, and p.T652P, and five combined mutations including p.[I66M + I289V], p.[I289V + I546T], p.[G270D + I546T], p.[G496S + I546T], and p.[G569S + I546T]. The sequences of all constructs were confirmed by DNA sequencing and restriction enzyme analysis.

2.6. Transfection and cell culture

COS1 cells were prepared to 70–80% confluence in 6-cm dishes on the day prior to transfection. Cell transfection was performed with 5 μL of TransFectin™ Lipid Reagent (Bio-Rad Laboratories K.K., Tokyo, Japan) and 8 μg of plasmids including empty vector (mock), wild-type *GALC* cDNA, and *GALC* mutant constructs. Transfection reaction was performed for 24 h and the medium was then changed to standard culture medium of Dulbecco's Modified Eagle Medium (Life Technologies Co., Carlsbad, CA) with 10% fetal calf serum for an additional 96 h. Finally, cells were harvested for enzyme activity measurement and Western blotting.

2.7. Measurement of GALC activity with HM-gal

Enzyme activity was measured with 6-hexadecanoylamino-4-methylumbelliferyl-β-D-galactopyranoside (HM-gal) (Slater & Frith

Table 1
Clinical information for 22 Japanese patients with Krabbe disease as newly reported in this study.

Patient no.	Age at onset	CSF protein (mg/dL)	MCV (m/s)	Abnormal GALC activity[a]	Phenotype	Genotype[b]	Polymorphic background
1	1 m	208	12	LYM (0)	Infantile	p.[R204X];[?]	289I/I 546I/T
2	3 m	ND	ND	LYM (0.1)	Infantile	c.[635_646delinsCTC];p.[T652P]	289I/I 546I/I
3	4 m	117	ND	LYM (0.2)	Infantile	p.[R204X];[?]	289V/V 546I/I
4	5 m	ND	ND	LYM (0.03)	Infantile	p.[G43R];[?]	289I/I 546I/T
5	5 m	ND	24	LYM (0.03)	Infantile	p.[W115X];[P302A]	289I/V 546I/I
6	6 m	194	16	LYM (0)	Infantile	**p.[Y341X];[Y341X]**	289I/I 546I/I
7	6 m	ND	ND	LYM (0.05)	Infantile	c.[635_646delinsCTC];[635_646delinsCTC]	ND
8	7 m	ND	ND	LYM (0)	Late-infantile	p.[G43R];[T652P]	289I/I 546I/T
9	8 m	148	Undetectable	LYM (0)	Late-infantile	p.[R204X];**c.[1808delT]**	289I/V 546I/I
10	10 m	ND	ND	LYM (0.1)	Late-infantile	**p.[L70P]**;[G270D]	289I/I 546I/T
11	11 m	52	Normal	LYM (0.1)	Late-infantile	c.[1719dupT];p.[L618S]	289I/I 546I/I
12	1 y and 2 m	62	ND	LYM (0.1)	Late-infantile	c.[1719dupT];p.[L618S]	289V/V 546I/I
13	1 y and 2 m	ND	ND	LYM (0.1)	Late-infantile	p.[I66M + I289V];[R204X]	289I/V 546I/I
14	2 y	ND	ND	LYM (0.1)	Late-infantile	p.[L618S];[?]	289I/I 546I/T
15	3 y	42	47	SF (0.2)	Juvenile	p.[P302A];[L618S]	289V/V 546I/I
16	14 y	ND	ND	LYM (0.4)	Adult	p.[L618S];[?]	289I/I 546I/T
17	20 y	ND	ND	LYM (0.2)	Adult	p.[A641T];[?]	289I/I 546I/T
18	35 y	ND	ND	SF (0.1)	Adult	p.[L618S];**[G646A]**	289I/I 546I/I
19	35 y	ND	ND	LYM (0.1)	Adult	p.[G43R];[I66M + I289V]	289I/V 546I/I
20	44 y	ND	55	LYM (0.05)	Adult	p.**[I289V + I546T]**;[?]	**289I/V 546I/T**
21	51 y	ND	ND	LYM (0.1)	Adult	p.[G270D];**[G352R]**	289I/V 546I/T
22	56 y	30	Normal	LYM (0.2)	Adult	p.[L618S];[?]	289I/I 546I/T

CSF, cerebrospinal fluid; GALC, galactocerebrosidase; m, month; LYM, lymphocyte; MCV, motor nerve conduction velocity; ND, not done; SF, skin fibroblast; y, year.
[a] *GALC activity is measured with HM-gal substrate and the normal GALC activity is >1 and >2 nmol/h/mg protein in lymphocytes and skin fibroblasts, respectively.*
[b] "?" indicates no mutation was found in the second allele and bold indicates a novel mutation.

Ltd, Norwich, UK) as an artificial fluorescence substrate following the Wiederschain protocol (Wiederschain et al., 1992). In short, harvested cells were sonicated and incubated with the substrate in citrate-phosphate (CP) buffer (pH 4.2) at 37 °C for 1 h and fluorescence (excitation at 385 nm/emission at 450 nm) was measured with a microplate reader. Enzyme activity was calculated as nmol/h/mg protein.

2.8. Measurement of GALC activity with [^{3}H]-GalCer

GALC activity was measured with [^{3}H]-galactocerebroside (GalCer) using the standard protocol (Suzuki, 1978). In short, cell lysate (70–80 μg/tube) was incubated with sodium tauorocholate (10 mg/mL) and oleic acid (2 mg/mL) with [^{3}H]-labeled GalCer in acidic media (CP buffer pH 4.2) at 37 °C for 1 h. Digested [^{3}H]-labeled galactose was separated from undigested GalCer with chloroform:methanol (2:1) extraction and radioactivity was measured. Enzyme activity was calculated as nmol/h/mg protein.

2.9. Measurement of GALC activity with [^{3}H]-psychosine

The psychosine degradation rate was measured with [^{3}H]-psychosine (American Radiolabeled Chemicals, Inc., St. Louis, MO) following a previously described protocol (Harzer et al., 2002; Miyatake and Suzuki, 1972). In short, cell lysate (70–80 μg/tube) was incubated with sodium tauorocholate (10 mg/mL), oleic acid (2 mg/mL), buffer A (50 mM Tris–HCl, 10 mM $MgCl_2$, and 8 mM mercaptoethanol) with [^{3}H]-labeled psychosine (25 μL/tube) (specific activity 44,000 dpm/nmol) in CP buffer (pH 4.5) at 37 °C for 24 h. After reaction, whole reaction sample was dried, extracted with methanol, and then subjected to thin layer chromatography (HPTLC silica gel 60; Merck-Millipore, Tokyo, Japan) to separate digested [^{3}H]-labeled galactose from undigested psychosine. The presence of digested [^{3}H]-galactose was confirmed by radioscanning, [^{3}H]-galactose containing silica gel was collected, and the radioactivity was measured. Enzyme activity was calculated as nmol/h/mg protein.

2.10. pH curve for mutant protein

CP buffers (0.1–0.2 M) were prepared at different pH (4–6) following standard protocol (Tanaka and Suzuki, 1976) and GALC enzyme activity was measured with HM-gal substrate for the COS1 cells transfected with common mutations (c.635_646delinsCTC, p.T652P, p.G270D, p.I66M + p.I289V, and p.L618S).

2.11. Heat stability for the mutant GALC protein

Cell lysate was incubated at 48 °C for 5 and 10 min with neutral CP buffer (pH 7). Enzyme activity was then measured with HM-gal substrate for c.635_646delinsCTC, p.T652P, p.G270D, p.I66M + p.I289V, and p.G569S.

2.12. Western blotting

Western blotting was performed as previously reported (Otomo et al., 2009). In short, whole cell lysate was mixed with sample buffer containing protease inhibitor and SDS. Samples (40 μg per lane) were applied to a 10% polyacrylamide gel. After SDS-PAGE, protein was transferred to a 0.45-μm PVDF membrane (Merck-Millipore) followed by blocking with 5% skim milk solution. Rabbit polyclonal anti-GALC antibody (51051-2-AP, Proteintech, Chicago, IL) was used at 1:3000 dilution as the primary antibody followed by the secondary antibody conjugated with horse radish peroxidase at 1:5000 dilutions. Detection was performed by chemical luminescence (SuperSignal West Dura; Thermo Fisher Scientific Inc., Tokyo, Japan).

2.13. Structural modeling of human wild-type and mutant GALC

A structural model of wild-type human GALC was built using molecular modeling software Modeller (http://salilab.org/modeller/) by means of homology modeling. The crystal structure of mouse GALC (PDB: 3ZR5) (Deane et al., 2011) was used as a template and energy minimization was carried out. The root-mean-square distance (RMSD) value was set at 0.05 kcal/mol/Å. The structural models of the mutant proteins incorporating amino acid substitutions were constructed using molecular modeling software TINKER (http://dasher.wustl.edu/ffe/) as previously described (Saito et al., 2012).

Coloring of the influenced atoms in the three-dimensional structures of the mutant GALC proteins was performed for the amino acid substitutions as to the distance between the wild-type and mutants to

Table 2
Clinical information for 29 previously reported Japanese patients with Krabbe disease.

Patient no.	Age at onset	Phenotype	Genotype[b]	Polymorphic background	Reference
23	3 m	Infantile	c.[635_646delinsCTC]; [635_646delinsCTC]	ND	Tatsumi et al. (1995)
24	4 m	Infantile	p.[T652P];[T652P]	289I/I 546I/I	Xu et al. (2006)
25	4 m	Infantile	c.[393delT];[?]	289I/I 546I/T	Xu et al. (2006)
26	4 m	Infantile	c.[635_646delinsCTC]; [635_646delinsCTC]	ND	Tatsumi et al. (1995)
27	4 m	Infantile	c.[635_646delinsCTC]; p.[T652P]	ND	Fu et al. (1999)
28	5 m	Infantile	p.[L364R];[T652P]	289I/V 546I/I	Xu et al. (2006)
29	5 m	Infantile	p.[R515H];[R515H]	ND	Fu et al. (1999)
30	<6 m	Infantile	p.[S52F];[W410G]	ND	Fu et al. (1999)
31	<6 m	Infantile	p.[R204X];[I234T]	289I/V 546I/I	Xu et al. (2006)
32	<6 m	Infantile	c.[635_646delinsCTC]; p.[R204X]	289I/V 546I/I	Xu et al. (2006)
33	6 m	Infantile	p.[W115X];[P302A]	289I/V 546I/I	Xu et al. (2006)
34	6 m	Infantile	c.[635_646delinsCTC]; [?]	289I/I 546I/T	Xu et al. (2006)
35	6 m	Infantile	c.[635_646delinsCTC]; p.[T652P]	289I/I 546I/I	Xu et al. (2006)
36	6 m	Infantile	p.[S257F];[?]	289I/I 546I/T	Xu et al. (2006)
37	8 m	Late-infantile	p.[P302A];[L618S]	289I/V 546I/I	Xu et al. (2006)
38	1 y	Late-infantile	c.[635_646delinsCTC]; p.[T262I]	ND	Fu et al. (1999)
39	2 y	Late-infantile	p.[G270D];[R515H]	289I/I 546T/T	Xu et al. (2006)
40	3 y	Juvenile	p.[I66M + I289V]; [W647X]	289I/V 546I/I	Xu et al. (2006)
41	3 y and 6 m	Juvenile	p.[I66M + I289V]; c.[1719dupT]	289I/V 546I/I	Xu et al. (2006)
42	3 y and 6 m	Juvenile	c.[635_646delinsCTC]; [?]	289I/I 546I/I	Xu et al. (2006)
43	5 y	Juvenile	c.[635_646delinsCTC]; p.[I66M + I289V]	289I/V 546I/I	Xu et al. (2006)
44	10–20 y	Adult	p.[G270D];[G270D]	ND	Furuya et al. (1997)
45	10–20 y	Adult	p.[I66M + I289V]; [I66M + I289V]	ND	Furuya et al. (1997)
45	10–20 y	Adult	p.[I66M + I289V]; [Y354X]	ND	Furuya et al. (1997)
47	10–20 y	Adult	p.[L618S]; [IVS6 + 5G>A]	ND	Furuya et al. (1997)
48	51 y	Adult	p.[L618S];[L618S]	ND	Satoh et al. (1997)
49	59 y	Adult	p.[I66M + I289V]; [I66M + I289V]	289V/V 546T/T	Xu et al. (2006)
50	60 y	Adult	p.[G496S];[G569S]	289I/I 546I/T	Tokushige et al. (2013)
51	69 y	Adult	p.[G270D];[G270D]	289I/I 546I/I	Xu et al. (2006)

m, month; y, year; ND, not done.
[b] "?" indicates no mutation was found in the second allele.

determine the influence of the amino acid substitutions geographically according to the method previously described (Saito et al., 2012).

2.14. Determination of root-mean-square distance (RMSD) values of all atoms and solvent-accessible surface area (ASA) values of amino acid residues

The RMSD values of all atoms in the mutant enzyme structures were determined according to Weiner's method to predict the severity of the structural changes as previously described (Weiner et al., 1984). To determine whether the amino acid substitutions are located in the protein core or on the protein surface, the ASA value of each amino acid residue in wild-type GALC was calculated using Stride (http://webclu.bio.wzw.tum.de/stride/).

2.15. Calculation of the numbers of atoms influenced by amino acid substitutions

To determine the influence of the amino acid substitutions on the GALC protein structure, each mutant model was superimposed on the wild-type GALC structure based on the α-C atoms. We defined that the structure was influenced by an amino acid substitution when the position of an atom in a mutant differed from that in the wild-type structure by more than 0.15 Å based on the total RMSD. The numbers of influenced atoms in the main chain and side chain were calculated.

2.16. Statistical analysis

Experiments were performed three times each in duplicate. Data presented are means ± standard error (SE). Comparison was conducted with a Student's *t*-test. Results were considered statistically significant when $p < 0.05$.

3. Results

3.1. Phenotypes of the patients in Japan

For the total cohort of 51 patients with Krabbe disease, the phenotypes regarding age at onset were infantile (n = 21, 41%), late-infantile (n = 10, 20%), juvenile (n = 5, 10%), and adult (n = 15, 29%) (Tables 1 and 2). Thus, 59% had late-onset Krabbe disease.

3.2. Novel mutations

We detected 36 mutant alleles for the 22 new patients and found five novel mutations including one small deletion c.1808delT, one homozygous nonsense mutation p.Y341X, and three heterozygous missense mutations p.L70P, p.G352R, and p.G646A (Table 1).

3.3. Detection of the 30-kb deletion

The 30-kb deletion was not found in patients 1, 3, 4, 14, 16, 17, 20, and 22, who only had one mutant allele.

3.4. Phenotype–genotype correlation

Ninety causative mutations (88%) were detected among the total cohort of 51 patients (102 alleles). The seven most common mutations including c.635_646delinsCTC, p.T652P, p.R204X, p.P302A, p.[I66M + I289V], p.L618S, and p.G270D were detected in 59 alleles (58%) out of 102 alleles. Four mutations, c.635_646delinsCTC, p.T652P, p.R204X, and p.P302A, were responsible for infantile-onset disease as patients who were homozygous or compound heterozygous for these mutations showed the infantile phenotype. Three mutations, p.[I66M + I289V], p.L618S, and p.G270D, contributed to late-onset disease as patients who were heterozygous for these mutations showed late-onset phenotypes (Table 3). By detecting two common infantile mutations or one common late-onset mutation in a patient, we can expect the phenotype to be infantile or late-onset in 16% and 45% patients, respectively. Phenotype can therefore be determined for a total of 61% of the patients by checking these seven common mutations.

3.5. Screening for the novel p.L70P, p.G352R, and p.G646A mutations in healthy subjects

The novel p.L70P, p.G352R, and p.G646A mutations were not detected in 100 healthy control subjects. These missense loci for the *GALC* gene

Table 3
Genotype–phenotype correlation for all mutations detected in Japanese Krabbe patients.

Mutation (new nomenclature)	Mutation (old nomenclature)	Phenotype				Total (%)
		Infantile	Late-infantile	Juvenile	Adult	
c.683_694delinsCTC	c.635_646delinsCTC	10	2	2	0	14 (13.7)
p.T668P	p.T652P	6	1	0	0	7 (6.8)
p.R220X	p.R204X	4	2	0	0	6 (5.8)
p.P318A	p.P302A	2	1	1	0	4 (3.9)
p.L634S	p.L618S	0	3	1	7	11 (10.7)
p.[I82M + I305V]	p.[I66M + I289V]	0	1	3	6	10 (9.8)
p.G286D	p.G270D	0	2	0	5	7 (6.8)
Sub-total						59/102 (58)
p.G59R	p.G43R	1	1	0	1	3 (2.9)
p.R531H	p.R515H	2	1	0	0	3 (2.9)
c.1767dupT	c.1719dupT	0	2	1	0	3 (2.9)
p.W131X	p.W115X	2	0	0	0	2 (1.9)
p.Y357X	p.Y341X	2	0	0	0	2 (1.9)
p.S68F	p.S52F	1	0	0	0	1 (1.0)
p.L86P	p.L70P	0	1	0	0	1 (1.0)
p.I250T	p.I234T	1	0	0	0	1 (1.0)
p.S273F	p.S257F	1	0	0	0	1 (1.0)
p.T278I	p.T262I	0	1	0	0	1 (1.0)
p.G368R	p.G352R	0	0	0	1	1 (1.0)
p.Y370X	p.Y354X	0	0	0	1	1 (1.0)
p.L380R	p.L364R	1	0	0	0	1 (1.0)
p.W426G	p.W410G	1	0	0	0	1 (1.0)
p.G512S	p.G496S	0	0	0	1	1 (1.0)
p.G585S	p.G569S	0	0	0	1	1 (1.0)
p.A657T	p.A641T	0	0	0	1	1 (1.0)
p.G662A	p.G646A	0	0	0	1	1 (1.0)
p.W663X	p.W647X	0	0	1	0	1 (1.0)
c.441delT	c.393delT	1	0	0	0	1 (1.0)
c.1856delT	c.1808delT	0	1	0	0	1 (1.0)
IVS6 + 5G>A	IVS6 + 5G>A	0	0	0	1	1 (1.0)
p.[I305V + I562T]	p.[I289V + I546T]	0	0	0	1	1 (1.0)
Total						90/102 (88)

Of the seven most common mutations (58% of alleles), c.635_646delinsCTC, p.T652P, p.R204X, and p.P302A are mostly responsible for the infantile phenotype while p.[I66M + I289V], p.L618S, and p.G270D are mostly responsible for late-onset phenotypes.

are well conserved in different species including monkey, dog, and mouse (Luzi et al., 1997).

3.6. GALC enzyme activities with different substrates

We prepared COS1 samples transfected with each expression construct and measured their GALC enzyme activities. With HM-gal as substrate, the enzyme activities for infantile-onset mutations (c.635_646delinsCTC, p.T652P) after mock subtraction were 0%, whereas those for the late-onset mutations (p.G270D, p.[I66M + I289V], and p.L618S) and polymorphisms (p.I66M, p.I289V, and p.I546T) were 4–20% and 42–46% of normal, respectively (Fig. 1A). With [^{3}H]-GalCer as substrate, the enzyme activities for infantile-onset mutations after mock subtraction were 0%, whereas those for the late-onset mutations and polymorphisms were 6–20% and 40–55% of normal, respectively (Fig. 1B). With [^{3}H]-psychosine as substrate, the enzyme activities for infantile-onset mutations c.635_646delinsCTC and p.Y341X after mock subtraction were 0% and 6% for p.T652P, whereas the late-onset mutations and polymorphisms showed 8–19% and 36–40% of normal, respectively (Fig. 1C). Novel or uncommon mutations, p.Y341X, p.L70P, p.G352R, and p.G496S, had no enzyme activities with HM-gal and [^{3}H]-GalCer, while p.G569S mutation had 11% activity with HM-gal and 9% with [^{3}H]-GalCer (Fig. 1A & B). The activities for each mutation were basically correlated with disease severity. Statistical analyses of the difference in activity between the common infantile-onset mutation c.635_646delinsCTC and late-onset mutations and polymorphisms were most significant when activities were measured with natural substrate or psychosine, although HM-gal was less hazardous and we measured maximum number mutations using this system.

3.7. GALC protein processing

The precursor 80-kDa protein band was detected for all the constructs except mock and the nonsense mutation p.Y341X, and there were no major differences between wild type and infantile or late-onset mutations. The processed 30-kDa protein band was well detected only with late-onset mutations (Fig. 1D). The uncommon and/or novel mutations (p.L70P, p.G352R, and p.G496S) had a weaker 30-kDa band than that for p.G569S (Fig. 1D). The 30-kDa bands were denser for p.I66M, p.I289V, p.I546T, and p.G270D alone. They were weaker for p.[I66M + I289V], p.[I289V + I546T], and p.[G270D + I546T] as combinations with p.I546T (Fig. 2C). p.G270D is a common late-onset mutation world-wide and its coincidence with p.I546T proved to influence residual activity. Heat treatment showed that both 80-kDa and 30-kDa protein bands remained intact except for p.G569S where the 30-kDa protein band was degraded after 10 min of heat treatment (Fig. 3C). It is not possible to detect the 50-kDa fragment with this antibody, although it is expected to show a similar expression pattern to the 30-kDa fragment.

3.8. Effect of polymorphism p.I546T on enzyme activity and GALC processing

The activity for p.G270D, p.G569S, p.G496S, and p.I289V was 20%, 11%, 0%, and 46% of normal, respectively, with HM-gal substrate, and 19%, 9%, 0%, and 55% of normal, respectively, with [^{3}H]-GalCer substrate after mock subtraction (Fig. 2A & B). However, when p.I546T was introduced with these mutations, activity was markedly lower. The activity of p.[G270D + I546T], p.[G569S + I546T], p.[G496S + I546T], and p.[I289V + I546T] mutations was 9%, 2%, 0%, and 16%, respectively,

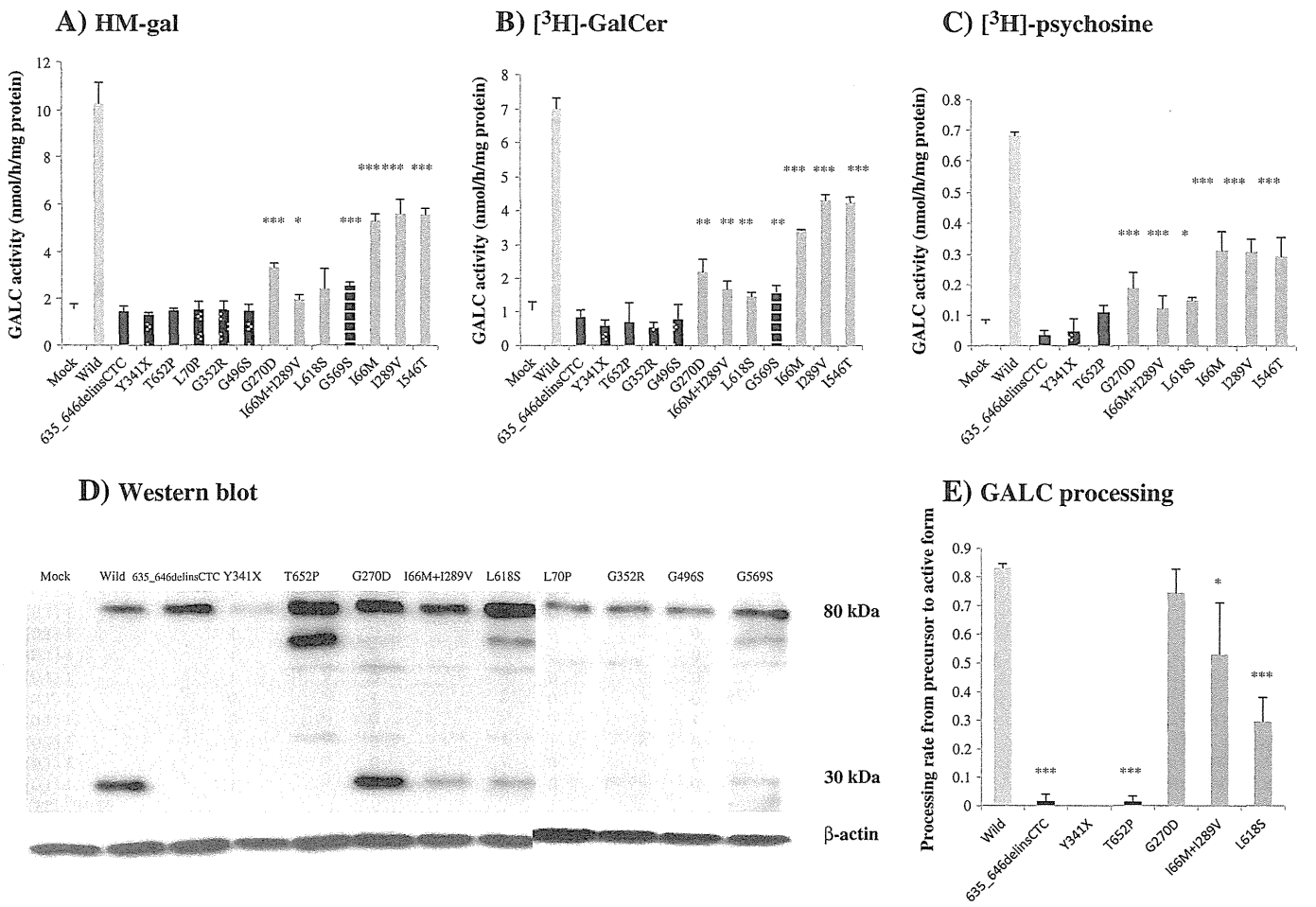

Fig. 1. *In vitro* expression of *GALC* mutations. Enzyme activities of transfected COS1 cells with wild type and mutants were measured with different substrates: A. HM-gal, B. [^{3}H]-GalCer, and C. [^{3}H]-psy (each n = 3). Common polymorphisms and late-onset mutants have higher activity than infantile mutants with all the substrates. Values are means ± SEM. *p < 0.05, **p < 0.01, and ***p < 0.005 [Student's *t*-test for all mutants and polymorphisms *vs.* c.635_646delinsCTC with all the substrates]. D. Western blotting of precursor (80 kDa) processing to GALC enzyme (30 kDa). All lanes except mock and stop codon mutant p.Y341X show precursor band, while processed protein is only observed for wild type and late-onset mutations. E. GALC processing rate is calculated by the ratio of 30-kDa to 80-kDa band densities (30 kDa/[30 kDa + {80 kDa/(80/30)}]) between wild type and mutations (each n = 3). Infantile-onset mutations show a low processing rate, while late-onset mutations show a high processing rate. Values are means ± SEM. *p < 0.05 and ***p < 0.005 (Student's *t*-test *vs.* wild type).

with HM-gal substrate, and 0%, 0%, 0%, and 7%, respectively, with [^{3}H]-GalCer substrate (Fig. 2A & B). In particular, p.[I289V + I546T], a combination of two polymorphisms, showed low activity as a late-onset mutant, p.[I66M + I289V]. On Western blotting, the precursor level of p.[I289V + I546T] was as faint as p.[I66M + I289V]. Taken together this combination p.[I289V + I546T] that is found in patient 20

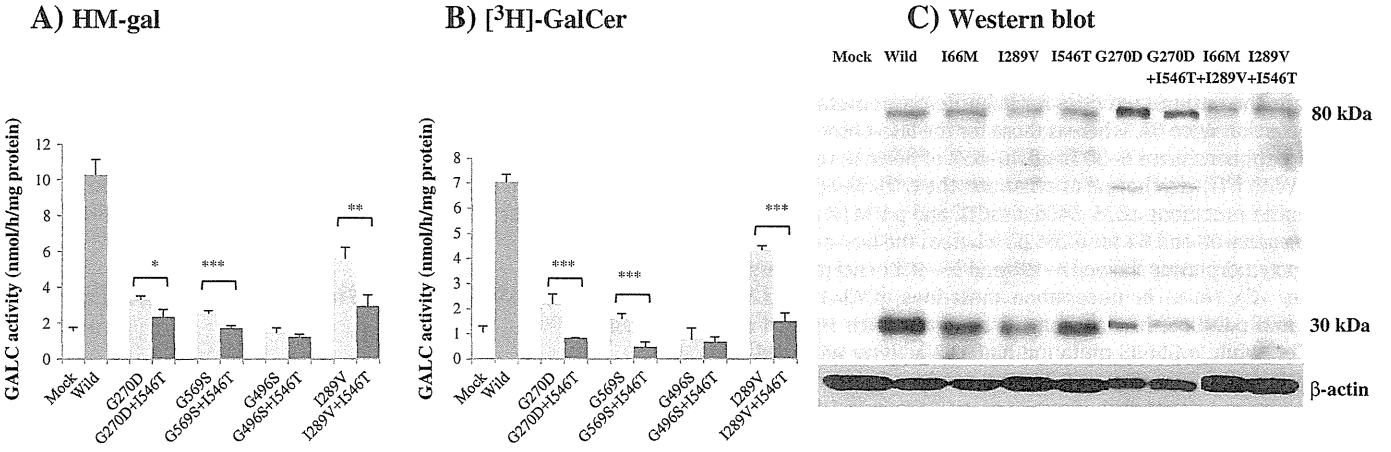

Fig. 2. *In vitro* effects of *GALC* polymorphisms and their combinations. GALC enzyme activity was measured for COS1 cells transfected with polymorphism p.I546T combined with different mutations with different substrates: A. HM-gal and B. [^{3}H]-GalCer (each n = 3). Presence of p.I546T causes reduced activity with both substrates. Values are means ± SEM. *p < 0.05, **p < 0.01 and ***p < 0.005 (Student's *t*-test). C. Western blotting shows that all three polymorphisms, p.I66M, p.I289V, and p.I546T, have a well processed 30-kDa band but combination of two polymorphisms causes a low processing rate.

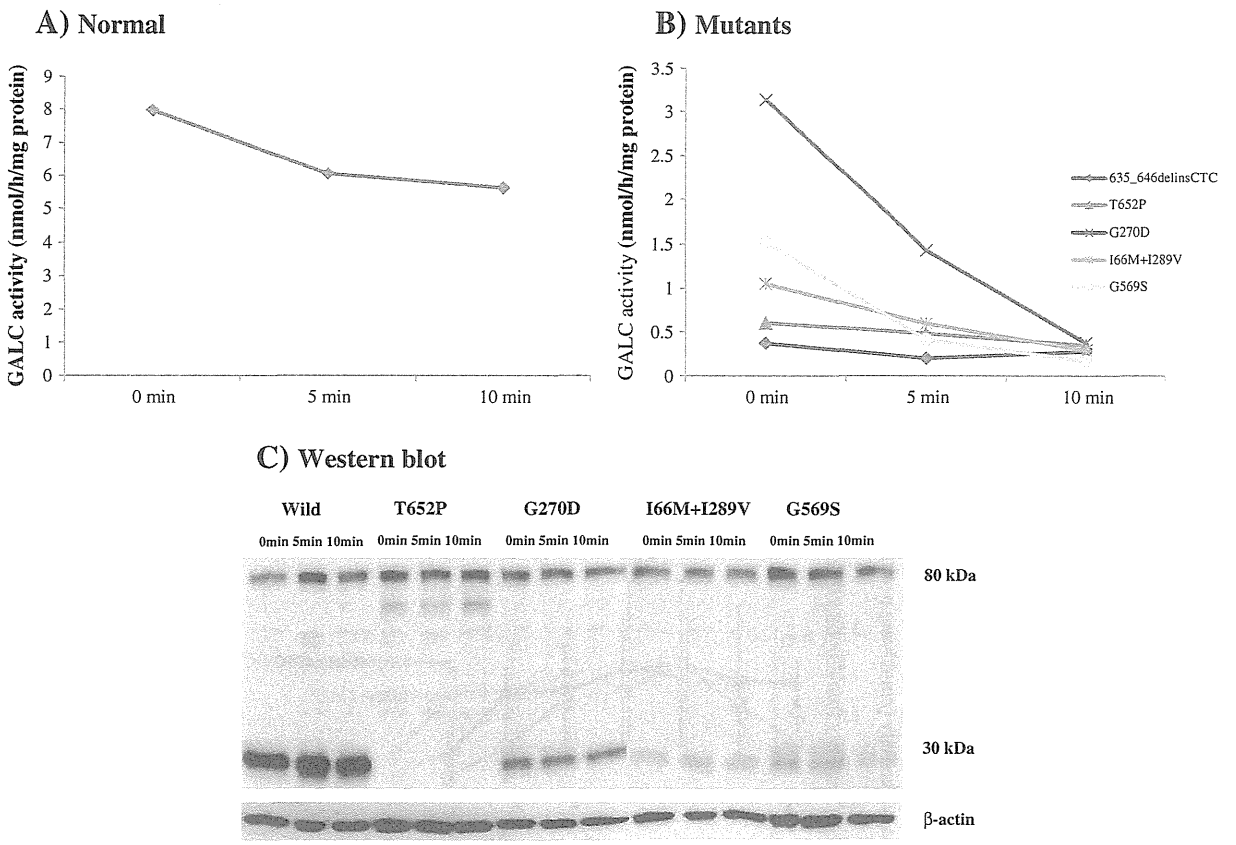

Fig. 3. Heat stability of wild-type and mutant GALC protein. After heat treatment at 48 °C, GALC activity was measured using HM-gal as a substrate. A. Wild-type GALC shows 75% and 70% stability after 5 and 10 min, respectively (mean; n = 2). B. All mutant proteins lost their activity after 5 min except for p.G270D, which had some activity (40%) after 5 min, but all lost activity after 10 min (mean; n = 2). C. Western blot shows both the precursor and processed protein remain intact except p.G569S for which processed protein (30 kDa) is degraded after 10 min.

(Table 1) is suggested as causative mutation such as p.[I66M + I289V]. This patient was diagnosed by clinical phenotype including early-onset dementia, dysarthria, spastic paraplegia, MRI image, and enzyme measurement.

3.9. pH curve for the mutant enzyme

Wild-type enzyme has maximal activity at pH 4.2 (Fig. 4A) as previously reported for the purified enzyme (Sakai et al., 1994b). The pattern of the pH curve appears different for the mutant enzymes. The activities for the mutants are lower and it was difficult to describe the precise optimal pH for each mutant (Fig. 4B and C).

3.10. Heat stability

For wild type, enzyme activity was reduced to 70% and 75% after 5 and 10 min of heat treatment, respectively (Fig. 3A). All the mutant proteins lost activity markedly after 5 min except for p.G270D, which maintained 40% activity after 5 min (Fig. 3B). The decrease in activity did not depend on the protein level as confirmed by Western blot (Fig. 3C).

3.11. Structural changes caused by the amino acid substitutions

A structural model of human GALC was constructed using crystallographic data for mouse GALC as a template. The amino acid identity between them was 83%. According to the constructed model, human GALC is composed of three domains: a β-sandwich domain, a central triosephosphate isomerase (TIM) barrel domain containing the active site, and a lectin domain. The locations of the amino acids involved in the substitutions examined in our study are shown in Fig. 5. They were distributed throughout the three domains comprising the enzyme molecule. The ASA values of the amino acids, for which substitutions are involved in Krabbe disease (p.L70P, p.G352R, p.G496S, p.G569S, and p.G646A) and GALC polymorphisms (p.I66M, p.I289V, and p.I546T) are 0.0–4.6 $Å^2$ and 0.0–0.8 $Å^2$, respectively. This suggests that the residues for Krabbe mutations are less solvent-accessible and located in the core region of GALC protein.

We constructed three-dimensional models of the mutant GALC proteins and calculated the RMSD values and numbers of affected atoms to predict the conformational changes due to the amino acid substitutions. Fig. 6 shows coloring of the influenced atoms in the three-dimensional structures.

- p.L70P: L70 exists at the end of an α-helix in the TIM barrel domain and is buried in the molecule. p.L70P is predicted to cause a moderate conformational change (Fig. 6A) and might decrease the stability of the protein.
- p.G352R: G352 is located on the β-sandwich domain and the structural change caused by p.G352R is predicted to be large. It should cause a large conformational change around the substituted residue (Fig. 6B).
- p.G496S and p.G569S: G496 and G569 are each located on the lectin domain and buried in the molecule. p.G496S (Fig. 6C) and p.G569S (Fig. 6D) are predicted to cause conformational changes near the boundary between the lectin and TIM barrel domains.
- p.G646A: G646 is located at the end of a loop in the lectin domain, being near a glycosylation site, and p.G646A is predicted to cause a conformational change around the substituted residue (Fig. 6E).

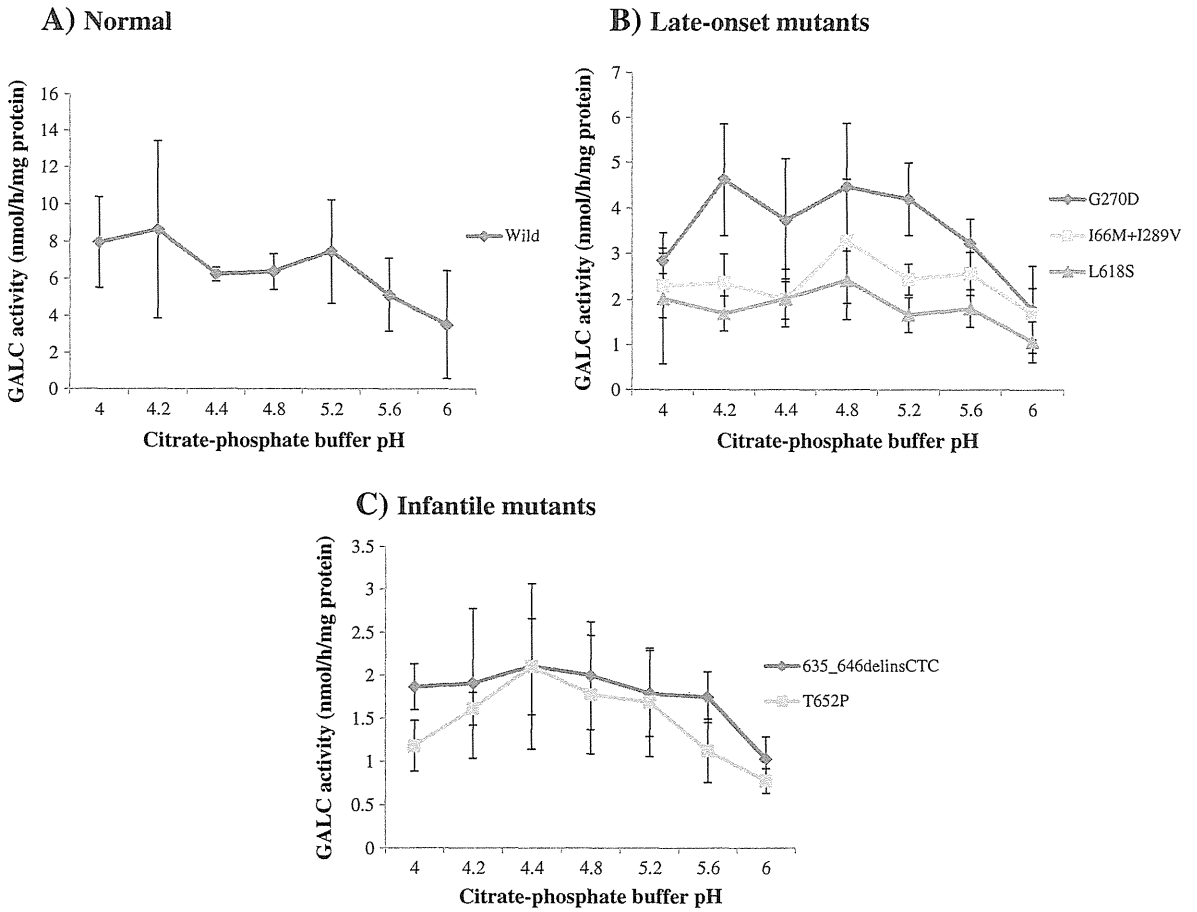

Fig. 4. pH curve for GALC activity for common mutation constructs. Enzyme activity was measured at different pH with HM-gal as substrate (each n = 3). Values are means ± SEM. A. Normal GALC showed higher activity at pH4.2. B. Late-onset mutation p.G270D had highest activity at pH 4.2 and other late-onset mutants showed highest activities at pH 4.8. C. Infantile mutants show highest activity at pH 4.4.

- p.I66M: I66 exists on an α-helix of the TIM barrel domain. p.I66M is predicted to affect conformation around the substituted residue (Fig. 6F).
- p.I289V: I289 is located on a β-strand of the TIM barrel domain. p.I289V is predicted to have little effect on the conformation of the protein (Fig. 6G).
- p.I546T: I546 is located on a β-strand of the lectin fold. p.I546T is predicted to cause a small conformational change around the substituted residue (Fig. 6H).
- p.I66M + P.I289V: The locations of I66 and I289 are distant (Fig. 6I). However, the resultant RMSD value and calculation of the number of affected atoms showed that coexistence of p.I66M and p.I289V causes a large conformational change (Table 4).
- p.I289V + p.I546T: The locations of I289 and I546 are distant (Fig. 6J). Their coexistence of p.I289V and p.I546T did not increase the RMSD value or the number of influenced atoms by the amino acid substitutions.

4. Discussion

With respect to clinical phenotype there are no especially specific features among Krabbe disease patients in Japan as compared to Caucasian patients (Debs et al., 2013). Common onset symptoms among late-onset patients in Japan are vision field impairment, spastic paraplegia, and learning difficulty. In addition, phenotype development is also very slow and it sometimes takes more than several years for patients or their families to notice the symptoms. Elderly patients with mild phenotypes can work until they retire with their symptoms only being recognized as part of the normal aging process.

In this study of the largest cohort of Japanese patients with Krabbe disease to date, we found that 59% of 51 patients had late-onset phenotypes of the disease, which is therefore the predominant phenotype in Japan. This is important information with respect to newborn screening in the future and applicability of potential treatment with bone marrow transplantation (BMT). BMT is the only established treatment option for Krabbe disease. As pre-symptomatic patients derive greater beneficial effects from BMT than symptomatic patients (Escolar et al., 2005) and because BMT is a very adverse treatment for newborn infants, newborns identified as having late-onset disease on screening can delay pre-symptomatic transplantation to an age more amenable for BMT. Our study provides a new protocol to classify novel mutations into infantile or late-onset forms by a combination of the transient expression methods using enzyme assay and Western blotting.

The *GALC* gene exhibits a high degree of molecular heterogeneity and most of the mutations are private mutations for which it is difficult to predict the phenotype. Newborn screening for Krabbe disease started in New York and they found it difficult to distinguish phenotypes by mutations (Duffner et al., 2009). In our study, we did not find the most frequent 30-kb deletion mutation for Caucasian patients. However, we were able to show a clear-cut relationship between the seven most common mutations and their phenotypes. If we find two alleles from four mutations (c.635_646delinsCTC, p.T652P, p.R204X, or p.P302A) in a homozygous or compound heterozygous state, the phenotype will be infantile-onset disease, while if we find one allele of the three mutations (p.[I66M + I289V], p.L618S, or p.G270D), the

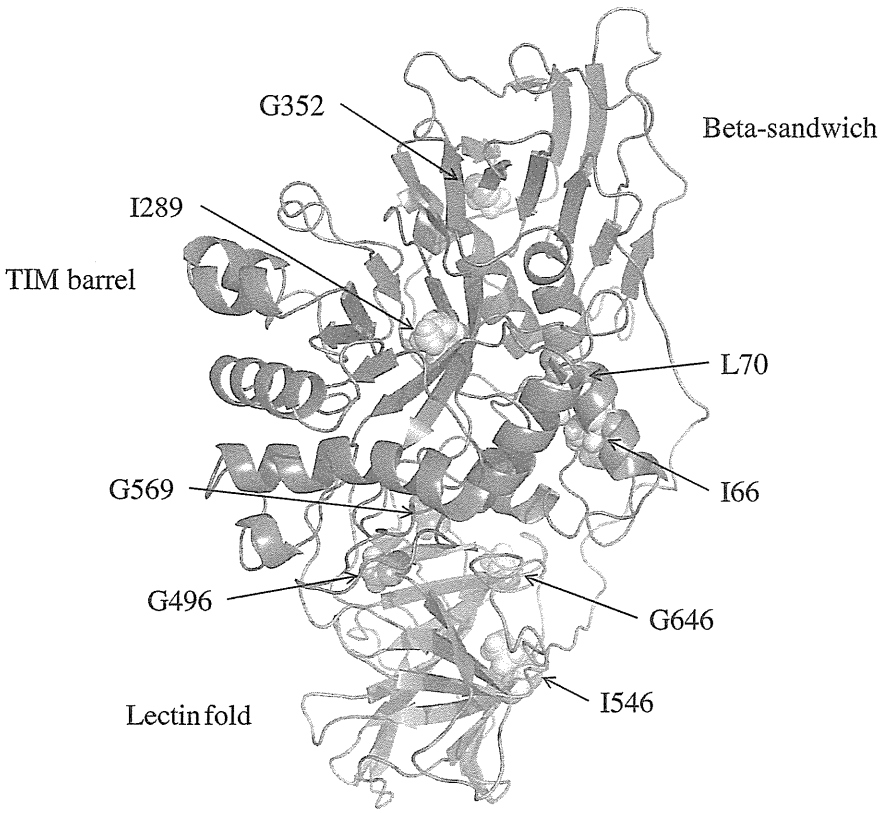

Fig. 5. Structural model of wild-type human GALC enzyme showing locations of the amino acids involved in the substitutions examined in this study. The backbone is shown as a ribbon. The residues involving substitutions are presented as space filling models.

phenotype will be late-onset phenotypes of disease without exception, at least in our Japanese cohort. This will therefore provide very useful information from the newborn screening of Krabbe disease in Japan with respect to treatment strategy.

Our study is the first to measure *in vitro* expression of GALC enzyme activity of mutation constructs using three different substrates, *i.e.*, fluorescent, natural, and psychosine substrates. We found significant differences between infantile-onset and late-onset mutations with all the substrates ($p < 0.05$ for HM-gal and $p < 0.01$ for [^{3}H]-GalCer and [^{3}H]-psychosine) and the difference between wild type, polymorphisms, and infantile-onset and late-onset mutations was well maintained with all the substrates (Fig. 3A, B, C). If we determine *in vitro* expression of GALC enzyme activity, we can therefore predict whether their phenotype will be infantile or late-onset by comparison with data for known common mutations. For example, patients 10 and 21 had one allele with a common late-onset mutation, p.G270D, which had high GALC activity, while the other allele was p.L70P or p.G352R, respectively, which had no GALC activity (Fig. 3A, B). As one allele had high residual activity, the phenotype remained mild. In patient 2, both alleles c.[635_646delinsCTC];p.[T652P] had no activities; the phenotype was therefore infantile. However, in patient 50, both alleles p.[G569S];[G496S] were unknown whereas one allele p.G569S had high activity and the other allele p.G496S had no activity from the experiment: the patient would therefore be expected to have a late-onset phenotype, which was confirmed in this report. We can now, therefore, predict phenotype as infantile and late-onset disease for all reported Krabbe patients: 61% patients can be diagnosed by screening the seven common mutations. The remaining patients can be predicted by determination of enzyme activity and mature protein expression with *in vitro* GALC expression.

On Western blotting, the processing rate of the GALC precursor (80 kDa) to active GALC (30 kDa) was also higher for late-onset mutations whereas infantile mutations had lower processing rates. Furthermore, the processing rate correlated well with GALC enzyme activity (Fig. 1E). This was also maintained for uncommon mutations.

The p.I546T polymorphism has a strong effect in reducing GALC activity when it is present with the other mutations (Fig. 2) and also has a strong effect on protein processing. In combination with another polymorphism, p.I289V, GALC activity is also reduced and protein processing is markedly inhibited. This is the first report of the p.[I289V + I546T] combination as a causative mutation.

The "psychosine hypothesis" was previously supported by the accumulation of psychosine in the brain (Svennerholm et al., 1980; Vanier and Svennerholm, 1976) and blood (Zhu et al., 2012), showing that disease severity is dependent on the amount of psychosine accumulation. Harzer et al. (2002) showed some correlations for phenotypes and psychosine degradation rate by using skin fibroblast and blood lymphocytes from patients who had compound heterozygous mutations. We have shown for the first time in this report with individual mutations that the severity of the mutation also correlates with the degradation of psychosine substrate. Late-onset mutations can degrade psychosine at a significantly higher rate than infantile mutations ($p < 0.005$) (Fig. 1C), which therefore supports the "psychosine hypothesis". Our experiments also indicate that high temperature reduces GALC activity for mutant GALC proteins (Fig. 3), which suggests a clinical insight for infantile patients who have a tendency to deteriorate under febrile conditions.

Enzyme structure analysis revealed that the infantile-onset mutation p.G352R causes a large structural change leading to a severe conformational change. The new mutation, p.G496S, is thought to affect the important core region of the enzyme molecule, although the structural change is small.

By mutation analysis and/or *in vitro* mutant GALC expression, we can separate all patients into two groups: infantile and late-onset phenotypes. However the late-onset phenotype cannot be divided in subgroups such as late-infantile, juvenile, or adult phenotypes. We need

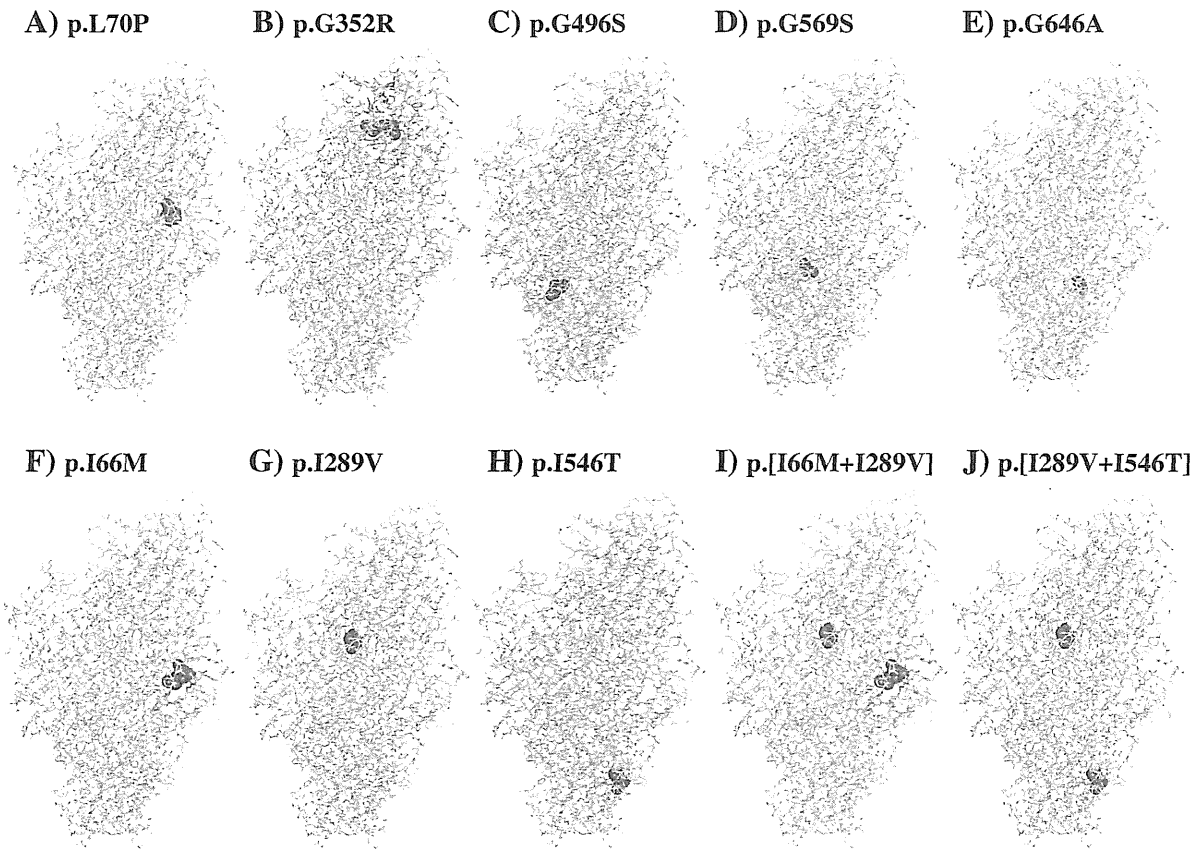

Fig. 6. Structural models of different mutant GALC enzymes. A. p.L70P, B. p.G352R, C. p.G496S, D. p.G569S, E. p.G646A, F. p.I66M, G. p.I289V, H. p.I546T, I. p.[I66M + p.I289V], and J. [p.I289V + p.I546T]. The distributions of the influenced atoms in the mutant GALC are shown. The colors of the atoms show the distances, as follows: blue < 0.15 Å, 0.15 Å ≤ cyan < 0.30 Å, 0.30 Å ≤ green < 0.45 Å, 045 Å ≤ yellow < 0.60 Å, 0.60 Å ≤ orange < 0.75 Å, and red ≥ 0.75 Å. The substituted amino acids are shown in the CPK model. (For interpretation of the references to color in this figure legend, the reader is referred to the web version of this article.)

to find some other alternative to classify all four phenotypes to select better treatment options. Our study provides a new protocol to classify novel mutations into infantile or late-onset forms by a combination of the transient expression method using enzyme assay and Western blotting. It takes considerable time to set up the methods for this expression system and to perform Western blotting, but it will be important to develop these systems in the future if the estimation of phenotype is eventually required during newborn screening.

It was long thought that mannose-6-phosphate is responsible for GALC transportation (Nagano et al., 1998). More recently, it has been suggested that the lectin domain, which is unique for the GALC protein structure, plays an important role in transportation (Deane et al., 2011). It has also been reported that some mutant GALC precursors cannot be transported to lysosomes and cannot be processed into active GALC, although infantile and late-onset mutations were not analyzed separately (Lee et al., 2010). This opens avenues for further study and we are now investigating the location of mutant GALC precursor, its transport, and site of degradation to active GALC for each phenotype.

Table 4
Conformational changes caused by *GALC* amino acid substitutions.

Amino acid substitution	Mutant characteristics	ASA (Å^2)	RMSD (Å)	No. of atoms affected	
				Main chain	Side chain
p.L70P	Krabbe; infantile	0	0.042	34	22
p.G352R	Krabbe; infantile	4.6	0.118	181	237
p.G496S	Krabbe; infantile	0	0.014	0	7
p.G569S	Krabbe; late-onset	0.2	0.034	32	25
p.G646A	Krabbe	1.5	0.03	10	3
p.I66M	Polymorphism	0	0.051	52	82
p.I289V	Polymorphism	0	0.005	0	0
p.I546T	Polymorphism	0.8	0.014	2	7
p.[I66M + I289V]	Krabbe; late-onset	0	0.066	89	149
p.[I289V + I546T]	Krabbe; possible late-onset	0.8	0.015	2	9

ASA, solvent-accessible surface area; RMSD, root-mean-square distance.

5. Conclusion

We summarize Japanese patients with Krabbe disease and report that the most common phenotype in Japan is the late-onset phenotype and not the infantile phenotype. We analyzed the common mutations in a transient enzyme expression system and found that enzyme activity using three substrates was correlated with that for the natural substrate and could be used to estimate clinical phenotype. Higher residual activity for late-onset mutations resulted from the higher processing rate of the mature enzymes.

Conflict of interest

All of the authors declare that there are no conflicts of interest.

Acknowledgments

This work was supported by Grants from the Ministry of Education, Culture, Science, Sports and Technology and the Ministry of Health,

Labour and Welfare of Japan. We thank Ms K. Tsujimoto for technical help with the experiments, which was very important for completion of the project.

References

Chen, Y.Q., Wenger, D.A., 1993. Galactocerebrosidase from human urine: purification and partial characterization. Biochim. Biophys. Acta 1170, 53–61.

Chen, Y.Q., Rafi, M.A., de Gala, G., Wenger, D.A., 1993. Cloning and expression of cDNA encoding human galactocerebrosidase, the enzyme deficient in globoid cell leukodystrophy. Hum. Mol. Genet. 2, 1841–1845.

De Gasperi, R., et al., 1996. Molecular heterogeneity of late-onset forms of globoid-cell leukodystrophy. Am. J. Hum. Genet. 59, 1233–1242.

Deane, J.E., et al., 2011. Insights into Krabbe disease from structures of galactocerebrosidase. Proc. Natl. Acad. Sci. U. S. A. 108, 15169–15173.

Debs, R., et al., 2013. Krabbe disease in adults: phenotypic and genotypic update from a series of 11 cases and a review. J. Inherit. Metab. Dis. 36, 859–868.

Duffner, P.K., et al., 2009. Newborn screening for Krabbe disease: the New York state model. Pediatr. Neurol. 40, 245–252.

Duffner, P.K., et al., 2012. Later onset phenotypes of Krabbe disease: results of the worldwide registry. Pediatr. Neurol. 46, 298–306.

Escolar, M.L., et al., 2005. Transplantation of umbilical-cord blood in babies with infantile Krabbe's disease. N. Engl. J. Med. 352, 2069–2081.

Fu, L., et al., 1999. Molecular heterogeneity of Krabbe disease. J. Inherit. Metab. Dis. 22, 155–162.

Furuya, H., et al., 1997. Adult onset globoid cell leukodystrophy (Krabbe disease): analysis of galactosylceramidase cDNA from four Japanese patients. Hum. Genet. 100, 450–456.

Harzer, K., Knoblich, K., Rolfs, A., Bauer, P., Eggers, J., 2002. Residual galactosylsphingosine (psychosine) β-galactosidase activities and associated GALC mutations in late and very late onset Krabbe disease. Clin. Chim. Acta 317, 77–84.

Kobayashi, S., Katayama, M., Satoh, J., Suzuki, K., Suzuki, K., 1988. The twitcher mouse. An alteration of the unmyelinated fibers in the PNS. Am. J. Pathol. 131, 308–319.

Lee, W.C., et al., 2010. Molecular characterization of mutations that cause globoid cell leukodystrophy and pharmacological rescue using small molecule chemical chaperones. J. Neurosci. 30, 5489–5497.

Lissens, W., et al., 2007. A single mutation in the GALC gene is responsible for the majority of late onset Krabbe disease patients in the Catania (Sicily, Italy) region. Hum. Mutat. 28, 742.

Luzi, P., Rafi, M.A., Wenger, D.A., 1996. Multiple mutations in the GALC gene in a patient with adult-onset Krabbe disease. Ann. Neurol. 40, 116–119.

Luzi, P., Rafi, M.A., Victoria, T., Baskin, G.B., Wenger, D.A., 1997. Characterization of the rhesus monkey galactocerebrosidase (GALC) cDNA and gene and identification of the mutation causing globoid cell leukodystrophy (Krabbe disease) in this primate. Genomics 42, 319–324.

Miyatake, T., Suzuki, K., 1972. Galactosylsphingosine galactosyl hydrolase: partial purification and properties of the enzyme in rat brain. J. Biol. Chem. 247, 5398–5403.

Nagano, S., et al., 1998. Expression and processing of recombinant human galactosylceramidase. Clin. Chim. Acta 276, 53–61.

Nagara, H., Ogawa, H., Sato, Y., Kobayashi, T., Suzuki, K., 1986. The twitcher mouse: degeneration of oligodendrocytes in vitro. Brain Res. 391, 79–84.

Otomo, T., Higaki, K., Nanba, E., Ozono, K., Sakai, N., 2009. Inhibition of autophagosome formation restores mitochondrial function in mucolipidosis II and III skin fibroblasts. Mol. Genet. Metab. 98, 393–399.

Puckett, R.L., et al., 2012. Krabbe disease: clinical, biochemical and molecular information on six new patients and successful retrospective diagnosis using stored newborn screening cards. Mol. Genet. Metab. 105, 126–131.

Saito, S., Ohno, K., Suzuki, T., Sakuraba, H., 2012. Structural bases of Wolman disease and cholesteryl ester storage disease. Mol. Genet. Metab. 105, 244–248.

Sakai, N., et al., 1994a. Krabbe disease: isolation and characterization of a full-length cDNA for human galactocerebrosidase. Biochem. Biophys. Res. Commun. 198, 485–491.

Sakai, N., et al., 1994b. Purification and characterization of galactocerebrosidase from human lymphocytes. J. Biochem. 116, 615–620.

Sakai, N., et al., 1998. Human galactocerebrosidase gene: promoter analysis of the 5′-flanking region and structural organization. Biochim. Biophys. Acta 1395, 62–67.

Satoh, J.I., et al., 1997. Adult-onset Krabbe disease with homozygous T1853C mutation in the galactocerebrosidase gene. Unusual MRI findings of corticospinal tract demyelination. Neurology 49, 1392–1399.

Seitelberger, F., 1981. Demyelination and leukodystrophy at an early age (in Spanish). Bol. Estud. Med. Biol. 31, 373–382.

Selleri, S., et al., 2000. Deletion of exons 11–17 and novel mutations of the galactocerebrosidase gene in adult and early-onset patients with Krabbe disease. J. Neurol. 247, 875–877.

Suzuki, K., 1978. Enzymic diagnosis of sphingolipidoses. Methods Enzymol. 50C, 456–488.

Suzuki, K., 1998. Twenty five years of the "psychosine hypothesis": a personal perspective of its history and present status. Neurochem. Res. 23, 251–259.

Svennerholm, L., Vanier, M.T., Månsson, J.E., 1980. Krabbe disease: a galactosylsphingosine (psychosine) lipidosis. J. Lipid Res. 21, 53–64.

Tanaka, H., Suzuki, K., 1976. Specificities of the two genetically distinct β-galactosidases in human sphingolipidoses. Arch. Biochem. 175, 332–340.

Tanaka, K., Nagara, H., Kobayashi, T., Goto, I., 1988. The twitcher mouse: accumulation of galactosylsphingosine and pathology of the sciatic nerve. Brain Res. 454, 340–346.

Tappino, B., et al., 2010. Identification and characterization of 15 novel GALC gene mutations causing Krabbe disease. Hum. Mutat. 31, 1894–1914.

Tatsumi, N., et al., 1995. Molecular defects in Krabbe disease. Hum. Mol. Genet. 4, 1865–1868.

Tokushige, S.I., et al., 2013. Isolated pyramidal tract impairment in the central nervous system of adult-onset Krabbe disease with novel mutations in the GALC gene. Brain Dev. 35, 579–581.

Vanier, M., Svennerholm, L., 1976. Chemical pathology of Krabbe's disease: the occurrence of psychosine and other neutral sphingoglycolipids. Adv. Exp. Med. Biol. 68, 115–126.

Weiner, S.J., et al., 1984. A few force field for molecular mechanical simulation of nucleic acid and proteins. J. Am. Chem. Soc. 106, 765–784.

Wenger, D.A., Rafi, M.A., Luzi, P., 1997. Molecular genetics of Krabbe disease (globoid cell leukodystrophy): diagnostic and clinical implications. Hum. Mutat. 10, 268–279.

Wenger, D.A., Rafi, M.A., Luzi, P., Datto, J., Costantino-Ceccarini, E., 2000. Krabbe disease: genetic aspects and progress toward therapy. Mol. Genet. Metab. 70, 1–9.

Wenger, D.A., Escolar, M.L., Luzi, P., Rafi, M.A., 2013. Scriver's The Online Metabolic and Molecular Bases of Inherited Disease (OMMBID). Chapter 147 Krabbe Disease (Globoid Cell Leukodystrophy). (Available at: http://www.ommbid.com/OMMBID/the_online_metabolic_and_molecular_bases_of_inherited_disease/b/abstract/Part16/ch147 [accessed 28 Oct 2013]).

Wiederschain, G., Raghavan, S., Kolodny, E., 1992. Characterization of 6-hexadecanoylamino-4-methylumbelliferyl-β-D-galactopyranoside as fluorogenic substrate of galactocerebrocidase for the diagnosis of Krabbe disease. Clin. Chim. Acta 205, 87–96.

Xu, C., Sakai, N., Taniike, M., Inui, K., Ozono, K., 2006. Six novel mutations detected in the GALC gene in 17 Japanese patients with Krabbe disease and new genotype–phenotype correlation. J. Hum. Genet. 51, 548–554.

Zhu, H., Lopez-Rosas, A., Qiu, X., Van Breemen, R.B., Bongarzone, E.R., 2012. Detection of the neurotoxin psychosine in samples of peripheral blood: application in diagnostics and follow up of Krabbe disease. Arch. Pathol. Lab. Med. 136, 709–710.

(神眼 29：303～309, 2012)

話題

先天代謝異常症と眼：Gaucher病の眼科所見と治療

成田　綾, 大野　耕策
鳥取大学医学部脳神経小児科

Gaucher Disease: Ocular Findings and Therapy

Aya Narita, Kousaku Ohno
Division of Child Neurology, Faculty of Medicine, Tottori University

要　約

先天代謝異常症の多くは眼合併症を認め，その診断に眼科評価は非常に重要である．Gaucher病は最も頻度の高いライソゾーム病であり，その初発症状として特徴的な眼所見(水平性衝動性眼球運動障害, saccadic initiation failure)を認める．現在，酵素補充療法が可能であり，中枢神経治療を目指した低分子療法(基質合成抑制療法，シャペロン療法)も研究されている事から，積極的に疑い診断を行う必要がある．

(神眼29：303～309, 2012)

Abstract

Ocular manifestations occur in various inborn errors of metabolism and play an important role in diagnosis. Gaucher disease is the most common lysosomal storage disease, and results in accumulation of the sphingolipid, glucosylceramide, in the reticuloendothelial system. Ocular manifestations of Gaucher disease include failure in voluntary horizontal saccadic initiation and the display of compensatory behaviors, such as head thrusting and blinking, early in the course of the disease. As therapeutic approaches become available, the need for early diagnosis is increasingly important.

(Neuro-ophthalmol Jpn 29: 303～309, 2012)

Key Words: Gaucher disease, horizontal saccadic initiation failure, enzyme replacement therapy (ERT), substrate reduction therapy, chaperone therapy

別刷請求宛先：成田綾　〒683-8504　鳥取県米子市西町36-1　鳥取大学医学部脳神経小児科
Reprint Requests to: Aya Narita, Division of Child Neurology, Faculty of Medicine, Tottori University, 36-1 Nishi-cho, Yonago, Tottori 683-8504, Japan

はじめに

多くの先天代謝異常症は眼症状を合併する事が知られ[1]，特徴的な眼症状は診断に重要である．個々の先天代謝異常症はまれだが，その全てを合わせると新生児800～2500人に1人が罹患するとされ[2,3]，日常診療で無縁な疾患ではない．また，酵素補充療法(enzyme replacement therapy; ERT)の開発により先天代謝異常症の1つであるライソゾーム病は6疾患(Gaucher病，Fabry病，Pompe病，ムコ多糖症Ⅰ型/Ⅱ型/Ⅵ型)が治療可能となり，早期診断・治療開始が良好な予後につながる事が明らかにされており，適切に診断していく事が求められる．本稿では，Gaucher病(GD)の神経眼科所見について述べた後，その治療について概説する．

Gaucher病(GD)；Overview

ライソゾームとは細胞内物質の分解を主な役割とする細胞内小器官で，その内部に60種以上もの酸性水解酵素を含み，糖蛋白質や糖脂質，ムコ多糖などの分解を行う．ライソゾーム病とは酵素の遺伝的欠損により分解基質が蓄積し発症する疾患の総称で，罹患臓器(中枢神経系，骨・軟骨，肝脾・網内系，結合組織)に進行性の機能障害を生じる．とりわけ中枢神経系は脆弱であり，多くのライソゾーム病で精神運動発達遅滞や退行，痙攣，不随意運動，歩行障害，眼合併症を呈する．

GDはライソゾーム病の中で最も発症頻度が高く，グルコセレブロシダーゼ(GBA)遺伝子変異に基づくβグルコセレブロシダーゼ活性の低下により，その基質であるグルコセレブロシドが蓄積する常染色体劣性遺伝病である．その3徴は肝脾腫，貧血・血小板減少，骨症状で，神経症状の有無と重症度により非神経型(1型)と神経型(2, 3型)に分類される．世界的には非神経型(1型)が大部分(94%)を占める[4]が，本邦では神経型(2+3型)が63%を占める[5]．2型は乳児期発症で，筋緊張亢進，後弓反跳，脳幹障害(呼吸障害，嚥下障害)，斜視，著明な肝脾腫を伴い，急速進行性の神経障害を呈する予後不良な型である．一方，3型は緩徐進行性の神経障害を呈する．3型にはサブタイプがあり，初発症状として眼症状(水平性衝動性眼球運動障害，眼球運動失行)が重要である．特に3b型は1型と同様の臓器蓄積症状に加え，水平性眼球運動障害を唯一の神経症状とする為[6,7]，1型との鑑別に難渋する．しかし1型はERTにてその予後が大きく改善するのに対し，3型ではその神経症状に対するERTの効果は乏しい為，予後を判断する上でも眼球運動の評価は重要である[8]．

GDと眼合併症

GDの眼合併症として眼球運動障害(水平性衝動性眼球運動障害，saccadic initiation failure)[6,8,9]や，眼底異常(preretinal and intraretinal white spots)[10,11]が知られる．

1. 眼球運動障害

神経型(2型+3型)GDでは眼球運動障害は71%に認められる[12]．発症年齢(中央値)は2歳で，水平性眼球運動障害が最も多く，smooth pursuitは速度が緩徐になる事もあるが，概ね保たれるのに対して，顕著にsaccadic initiationが障害される為に眼球運動失行を呈する．Supranuclear gaze palsy[6,13]と記載されるが，個々の症例を検討するとその多くはsaccadic initiationの障害である様に思われる．head thrustingは眼球運動失行の特徴的な所見だが神経型GDでは約半数にしか認められず[12,14]，代わりに眼球運動直前の瞬目(blinking)や眼球を弓状に上転させなが